



1 **The diurnal cycle of cloud profiles over land and ocean between 51°S and 51°N, seen by**
2 **the CATS spaceborne lidar from the International Space Station**

3

4 Vincent Noel ¹, H el ene Chepfer ², Marjolaine Chiriaco ³, John Yorks ⁴

5

6 1 - Laboratoire d'A erologie, CNRS/UPS, Observatoire Midi-Pyr en ees, 14 avenue Edouard
7 Belin, Toulouse, France

8 2 - LMD/IPSL, Sorbonne Universit e,  cole polytechnique,  cole Normale Sup erieure, PSL
9 Research University, CNRS, F-91120 Palaiseau, France

10 3 - LATMOS/IPSL, Univ. Versailles Saint-Quentin en Yvelines, France

11 4 - NASA GSFC, Greenbelt, Maryland, USA

12

13 Proposed for publication in:

14 Atmospheric Chemistry and Physics

15

16 23 Mar 2018

17



18 **Abstract.**

19 We take advantage of 15 months of measurements from the Cloud and Aerosol Transport
20 System (CATS) lidar on the non-sun-synchronous International Space Station (ISS) to
21 document, for the first time, the diurnal cycle of detailed vertical profiles of Cloud Fraction
22 between 51°S and 51°N. After processing CATS lidar data, we analyzed the diurnal cycles of
23 the cloud profiles over ocean and over continent in two different seasons.

24 Over the Tropical ocean in summer, the high clouds geometric thickness increases
25 significantly from 1km near 5PM to 5km near 10PM, resulting in a high clouds maximum at
26 nighttime. Over the summer tropical continents, CATS observations reveal the presence of a
27 mid-level cloud layer (4-8 km ASL) persisting all-day long, with a weak diurnal cycle
28 (minimum at noon). Over the Southern Ocean, diurnal cycles appear for the omnipresent
29 low-level clouds (minimum between noon and 3PM) and for the high-altitude clouds
30 (minimum between 8AM and 2PM). Both cycles are time-shifted, with high-altitude clouds
31 following the changes in low-altitude clouds by several hours. Over all continents at all
32 latitudes during summer, the low-level clouds develop vertically and reach a maximum
33 occurrence at about 2.5 km ASL in the early afternoon (around 2 pm).

34 Our work also show that 1) the diurnal cycles of vertical profiles derived from CATS are
35 consistent with those from ground-based active sensors at local scale, 2) the cloud profiles
36 derived from CATS measurements at local times of 0130AM and 0130PM are consistent
37 with those observed from CALIPSO at similar times, 3) the diurnal cycles of low and high
38 cloud amounts derived from CATS are in general in phase with those derived from
39 geostationary imagery but less pronounced. Finally, the diurnal variability of cloud profiles
40 revealed by CATS strongly suggests that CALIPSO measurements at 0130AM and PM
41 document the daily extremes of the cloud fraction profiles over ocean and are more
42 representative of daily averages over land, except at altitudes above 10km where they
43 capture part of the diurnal variability. These findings are equally applicable to other
44 instruments with local overpass times similar to CALIPSO's, like all the other A-Train
45 instruments and the future Earth-CARE mission.

46

47



48	Outline
49	1. Introduction
50	2. Data and methods
51	2.1 Data
52	a. Cloud detections from the CATS spaceborne Lidar
53	b. Cloud detections from ground-based active instruments
54	c. Cloud detections from passive and active spaceborne sensors
55	2.2 Methods
56	a. Building the diurnal cycle of Cloud Fraction profiles from lidar cloud detections
57	b. Building the diurnal cycle of Low and High Clouds Amounts from CATS data
58	3. Results
59	3.1 Diurnal cycle of Cloud Fraction profiles observed at Global scale
60	3.2 Diurnal cycle of Cloud Fraction profiles observed over mid-latitudes and Tropics
61	a. High clouds
62	b. Low clouds
63	c. Seasonal differences
64	3.3 Diurnal cycle of Cloud Fraction profiles above selected continental regions
65	a. Over South of Paris in Europe
66	b. Over the US Southern Great Plains ARM site
67	c. Over continents
68	4. Discussion
69	4.1 About the diurnal cycles of the Low and High Cloud Amounts
70	4.2 About the Cloud Fraction profiles observed at fixed local times by space lidars
71	5. Conclusions
72	



73 **1. Introduction**

74 Cloud cover diurnal cycles have been documented from space by geostationary satellites as
75 early as the late 1970's (e.g. Gray and Jacobson, 1977) and were summarized based on
76 retrievals from the International Satellite Cloud Climatology Project (ISCCP; Cairns, 1994;
77 Rossow and Schiffer, 1999). Soden (2000) and Tian et al. (2004) used those retrievals to
78 confront the diurnal cycles of clouds, convective activity and water vapor in the upper
79 troposphere, pointing to a clear land-sea contrast. More recently, Philippon et al. (2016)
80 used MSG-SEVIRI data to describe the diurnal variations in the composition of cloud cover
81 above Central Africa. Taylor et al. (2017) also used MSG-SEVIRI to describe when during the
82 day the cloud top temperature is the coldest on average seasonally, over a half-hemisphere
83 grid. Apart from geostationary imagery, few spaceborne instruments provide a sampling
84 frequency well-suited to describe the diurnal variability of clouds. For instance, Wylie (2008)
85 had to take advantage of the four observations per day provided by the NOAA series of
86 polar orbiters to document a weakly-resolved clouds diurnal cycle from multispectral
87 infrared data.

88 Those studies found the most significant diurnal changes of clouds over continents in
89 summer: low-level boundary layer clouds expand throughout the day, following the
90 warming of the surface by incoming solar radiation, a process significantly affected by
91 orography. In the Tropics, this near-surface activity is transmitted to higher altitudes
92 through deep convection, driving a diurnal cycle in high-level clouds. The time needed for
93 this process to occur delays the cycle of high clouds, whose maximas and minimas occur
94 hours late compared to low-level clouds. At midlatitudes, without deep convection most of
95 the troposphere is free from surface influence, and diurnal changes in the distribution of
96 high-altitude clouds are rather driven by the local atmospheric circulation (e.g. Storm-
97 tracks), leading to less predictable patterns. Over oceans, the largest low-level cloud covers
98 happen in the morning, when the expansion generated by nighttime radiative cooling at
99 cloud top stops. These patterns are supported by understood physical principles and are
100 well documented by passive satellite imagery. But these observations do not provide
101 information on the diurnal cycle of the detailed cloud profiles, which is key to better
102 understand the atmospheric heating rate profile.



103 Active remote sensing instruments, such as radars and lidars, document the cloud vertical
104 distribution with greater accuracy resolutions than passive instruments, with vertical
105 resolutions finer than 500m. For decades, active instruments have been operated from
106 ground-based sites, building extensive datasets from which time series and statistics about
107 clouds can be derived (e.g. Noel et al., 2006). From space, Liu and Zipser (2008) were able to
108 derive information on the clouds diurnal cycle from the spaceborne Tropical Rainfall
109 Measuring Mission radar, launched in 1997 (Kummerow et al., 1998), but the instrument
110 was not designed to detect clouds with accuracy. The CALIPSO lidar (Cloud-Aerosol Lidar
111 and Infrared Pathfinder Satellite Observations), since its launch into orbit in 2006 (Winker et
112 al., 2010), has provided transformative vertically-resolved data on clouds (Stephens et al.,
113 2017; Winker et al., 2017). Enhanced cloud detections from CALIPSO have, among other
114 things, helped pinpoint and improve significant cloud-related weaknesses in climate models
115 (e.g. Cesana and Chepfer, 2013; Konsta et al., 2016), helped improve estimates of the
116 surface radiation budget (Kato et al., 2011) and of the heating rate profile (L'Ecuyer et al.,
117 2008; Haynes et al., 2013; Bouniol et al., 2016). However, due to its sun-synchronous polar
118 orbit CALIPSO samples the atmosphere at either 1:30AM or 1:30PM local time (LT). The
119 CloudSat radar (Stephens and Kummerow, 2007) and all A-Train instruments (L'Ecuyer and
120 Jiang, 2010) share the same overpass times. Even though measurements limited to two
121 times of day can still offer insights into the day-night cloud changes (Sèze et al., 2015; Gupta
122 et al., 2018), they are insufficient to fully document the diurnal evolution of cloud profiles.
123 This observational blind spot explains why very little is known so far about how the vertical
124 distribution of clouds changes diurnally in most of the globe.

125 Here we take advantage of measurements from the Cloud Aerosol Transport System (CATS,
126 McGill et al., 2015) lidar on the International Space Station (ISS), to document the diurnal
127 evolution of the vertical distribution of clouds in regions of the globe. The CATS dataset is
128 unique so far, as it contains active vertically-resolved measurements made by lidar from
129 space with variable local times of overpass: the CATS lidar can document cloud profiles at
130 different times along the day between 51°S and 51°N following the ISS orbit.

131 We first describe how data were selected and processed to derive diurnal cycles of cloud
132 Cloud Fraction profiles and Cloud Amounts from CATS and all other instruments included for
133 comparison (Sect. 2). Then, using CATS retrievals we document, for the first time, the



134 diurnal cycle of detailed Cloud Fraction profiles in large regions of the globe in two seasons
135 over ocean and land (Sect. 3.1 and 3.2). In Sect. 3.3 we describe CATS-derived diurnal cycles
136 of cloud profiles over selected sites and continents with two goals in mind: (i) to compare
137 them with independent ground-based observations to check the validity of the CATS
138 retrievals, and (ii) to document the diversity of the continental cloud profile diurnal cycles
139 over the globe. In Section 4 we discuss implications of our results: We compare the diurnal
140 cycle of the Low and High cloud covers derived from CATS with ones from geostationary
141 satellites (Sect. 4.1), and discuss the agreement between CATS Cloud Fraction profiles
142 derived at the times of CALIPSO overpass with actual CALIPSO retrievals (Sect. 4.2.a). Finally,
143 we consider CATS profiles at overpass times from current and future sun-synchronous
144 spaceborne lidar missions (Sect. 4.2.b) to understand which part of the diurnal cloud cycle is
145 sampled by these instruments. We conclude in Sect. 5.



146 **2. Data and Methods**

147

148 **2.1 Data**

149

150 ***a) Cloud detections from the CATS spaceborne lidar***

151 In this study our primary data consist of cloud detected during June-July-August (JJA) and
152 December-January-February (DJF) periods using data from the CATS lidar system (Yorks et
153 al., in preparation). CATS operated from the ISS between February 2015 to late October
154 2017. Although CATS was originally designed to operate at 3 wavelengths (355, 532 and
155 1064nm) with variable viewing geometries, beginning in March 2015 technical issues limited
156 operation to a single 1064nm wavelength and a single viewing mode. The CATS instrument
157 went on providing single-channel high-quality data (Yorks et al., 2016a) until a fault in the
158 on-board power and data system ended science operations on October 30, 2017.

159 Being located on the ISS means measurements from CATS are constrained to latitudes
160 below 51°, giving it access to ~78% of the Earth's surface. This however prevents our study
161 from covering polar regions. However, this leads to densely distributed overpasses at
162 latitudes above 40°: CATS sampling is particularly good in populated midlatitude regions and
163 above the Southern Ocean.

164 CATS cloud detections were derived from vertical profiles of ATtenuated Backscatter
165 measured every 350m at 1064nm with a 60m vertical resolution. ATB profiles were
166 calibrated, processed and averaged based on the procedures designed for CALIOP data to
167 enable threshold-based cloud detection (Yorks et al., 2016b and in preparation). Unlike for
168 CALIOP, the cloud detection algorithms for CATS rely primarily on 1064nm data. They create
169 the CATS operational Level 2 (L2) products, which provide properties for detected clouds
170 (including base and top) every 5km along-track. Hereafter we used such cloud properties
171 from CATS L2O data files v2.01 (Palm et al., 2016), including only layers with a
172 Feature_Type_Score above 5, to avoid including wrongly-classified optically thick aerosol
173 layers near deserts. To document the diurnal cycle (Sect. 2.2.a), we used data obtained in
174 both nighttime and daytime (sunlit) conditions between March 2015 and October 2017.



175 CATS cloud data being still novel at the time of this writing, we document and discuss
176 several of its characteristics in Appendices A and B, including sampling variability and the
177 sensitivity of cloud detection in presence of solar pollution. This exploration of CATS data
178 (and the upcoming comparisons with other instruments) made us confident that its
179 sampling and cloud detections are robust enough to be used for scientific purposes.

180

181 ***b) Cloud detections from ground-based active instruments***

182 Like with any lidar, the CATS laser beam gets fully attenuated when passing through clouds
183 with optical depths larger than typically 3 (e.g., Chepfer et al., 2010). This can lead to the
184 cloud fraction being underestimated in the lower troposphere. To estimate how much the
185 CATS cloud fraction is biased at low altitudes, we compare CATS detections with
186 independent observations collected from ground-based active instruments.

187 Ground-based observation sites provide long-term records of atmospheric properties over
188 periods that often cannot be reached by satellite instruments (Chiriaco et al., in revision).
189 Nowadays such sites are often well equipped with active remote sensing instruments. Data
190 acquisition, calibration and processing are often homogenized in the framework of specific
191 observation networks (e.g. EARLINET, the European Aerosol Research Lidar Network,
192 Pappalardo et al., 2014). Descriptions of the clouds diurnal cycle based on ground-based
193 measurements are however scarce. In this study, we compare CATS cloud cycles with those
194 derived from active measurements at two ground-based sites in Europe and the United
195 States.

196 The first ground-based site is the Site Instrumenté de Recherche par Télédétection
197 Atmosphérique (SIRTA, Haefelin et al., 2005), 20km South-West of Paris at 48.7°N, 2.2°E.
198 From SIRTA we used observations from the Lidar Nuages et Aérosols (LNA, Elouragini and
199 Flamant, 1996). Cloud detections from the LNA were homogeneized, repackaged and made
200 available in the framework of the SIRTA-reOBS project (Chiriaco et al., 2014; Chiriaco et al.,
201 in revision). The LNA requires human supervision and does not operate under precipitation,
202 leading to irregular sampling and almost no nighttime measurements. Its long operation
203 time however means its dataset covers almost 15 years. Cloud layers were detected in LNA
204 profiles of attenuated backscatter following a threshold-based approach similar to CATS and



205 CALIPSO.

206 The second site we consider is the Atmospheric Radiation Measurement (ARM) Southern
207 Great Plains (SGP) site, at 97°W, 36°N. From this ground-based site we consider cloud
208 retrievals from the Millimeter Wavelength Cloud Radar (MMCR) and from the Raman Lidar
209 (RL). The MMCR has been routinely operated to detect and identify clouds and
210 precipitations since 1996 (Moran et al., 1998), while RL cloud detections are available since
211 1998 (Ackerman and Stokes, 2003). In the framework of the present study we did no specific
212 processing of data from these instruments. Instead, we compare CATS cloud retrievals over
213 the SGP site with the descriptions made by Zhao et al. (2017, Fig. 3a) and Dupont et al.
214 (2011, Fig. 3) of the diurnal cycle of clouds over SGP based on 14 years of MMCR cloud
215 detections and 10 years of RL cloud detections in Sect. 3.3.

216

217 ***c) Cloud detections from passive and active spaceborne sensors***

218 In addition to the CATS, LNA and MMCR datasets, in the upcoming sections we use cloud
219 retrievals from two spaceborne datasets to put CATS cloud retrievals into a referenced
220 context. First, we consider the baseline reference for the description of the clouds diurnal
221 cycle from space: the analysis of data from the ISCCP done by Rossow and Schiffer (1999),
222 hereafter RS99. Their results are based on aggregated and homogenized infrared and visible
223 radiances from imaging radiometers on the international constellation of weather satellites.
224 They are widely considered as the reference for describing the diurnal cycle of the cloud
225 cover at large scales from space measurements. Like with SGP data, we did not reprocess
226 any ISCCP data for the present study, instead we rely on the description of the diurnal cycle
227 of low and high clouds RS99 documented in their Fig. 11 based on ISCCP, to which we
228 confront CATS retrievals in Sect. 4.1.

229 Finally, we also confront CATS cloud detections with retrievals based on measurements
230 from the CALIOP lidar, routinely made since 2006 from the sun-synchronous CALIPSO
231 platform at 13:30 and 01:30 LT in Sect. 4.2. To enable comparison with CATS retrievals, we
232 used cloud layers retrieved from CALIPSO measurements during the period of CATS
233 operation (March 2015 to October 2017), and documented at 5km horizontal resolution in
234 CALIPSO Level 2 V4.10 Cloud Layer Products (Vaughan et al., 2009). We processed both



235 CATS and CALIPSO data alike as described in Sect. 2.2.a.

236

237

238 **2.2. Methods**

239

240 ***a) Building the diurnal cycle of Cloud Fraction profiles from lidar cloud detections***

241

242 Analyzing CATS lidar echoes lets one identify at which altitude a cloud is present above a
243 particular location on Earth at a given moment. By aggregating such information over a long
244 period, vertical profiles of Cloud Fraction (CF) can be derived. A CF(z) profile documents at
245 which frequency clouds were observed at the altitude z over a particular location. Cloud
246 Fractions are conceptually equivalent to the Cloud Amounts derived from passive
247 measurements (next section), but vertically resolved with a 60 meters resolution.

248 From CATS level 2 data files, we extract profile-based cloud detections and use the
249 measurement UTC time and coordinates to deduce their local time of observation. Using the
250 resulting list of cloud layer altitudes, coordinates and local times of detection, we count the
251 number n of cloud detected within half-hour bins of local time, $2^\circ \times 2^\circ$ lat-lon boxes and
252 200m altitude bins. We also count the number of valid data points n_0 within those bins.

253 Eventually we derive the Cloud Fraction $CF = \frac{n}{n_0}$, either in individual local time/lat-

254 lon/altitude bin or by aggregating n and n_0 over a selection of bins.

255 CATS reports cloud layers as opaque when no echo from the surface is found in the profile
256 below a detected cloud, following the same methodology as in Guzman et al., 2017. Below
257 an opaque cloud layer, there is no laser signal left to propagate, and clouds potentially
258 present at lower altitudes will not be sampled by the lidar. To account for this effect, we
259 consider the portions of profiles below an opaque layer unsampled, and they do not count
260 in the number of valid data points n_0 . This approach limits the influence of laser attenuation
261 on cloud detections but cannot totally cancel it.

262 To enable comparisons with CATS CF profiles (Sect. 3.3 and 4.2), we followed a similar
263 approach to build CF profiles using cloud detections from SIRTA-reOBS (Sect. 2.1.b) and



264 from CALIPSO Level 2 products (Sect. 2.1.c). In both cases, we counted the number of cloud
265 detections and valid (non-attenuated) measurements in hourly local time bins and 200m
266 altitude bins. For CALIPSO, only 01:30AM and PM time bins were filled.

267

268 ***b) Building the diurnal cycle of Low and High Cloud Amounts from CATS data***

269

270 As ISCCP data are based on radiances, clouds therein are characterized according to
271 their retrieved top pressure P as low ($P > 680\text{hPa}$), middle ($440 < P < 680\text{hPa}$) or high
272 ($P < 440\text{hPa}$). To enable a direct ISCCP-CATS comparison, we derived Cloud Amounts (CA)
273 from CATS data for low and high clouds as defined by altitude: low clouds have their base
274 below 4km ASL, high clouds have tops above 7km, and mid-level clouds are in between.
275 Using the list of cloud layer altitudes, coordinates and local times of detection derived from
276 CATS detections (Sect. 2.2.a), we count the number of occurrences n' of at least part of one
277 cloud layer in half-hour bins of local time, $2^\circ \times 2^\circ$ lat-lon boxes and the three altitude ranges
278 (0-4km, 4-7km and higher than 7km ASL). We also count the number of occurrences n'_0 that
279 could possibly be reported given the measurements sampled by CATS within each bin,
280 taking into account the existence of opaque layers. Eventually, we derive the Cloud Amount
281 $CA = \frac{n'}{n'_0}$ for low, mid and high-altitude clouds layers, either in individual local time/lat-lon
282 bin or by aggregating n' and n'_0 over a selection of bins. Like RS99, we separated CATS cloud
283 detections over land and ocean, based on the International Geosphere-Biosphere
284 Programme surface flag present in CATS L2 products on a profile basis (Palm et al., 2016).



285 **3. Results**

286 **3.1. Diurnal Cloud fraction profiles observed at Global scale**

287

288 Figure 1 shows the global diurnal cycle revealed by CATS data over Ocean and Land during
289 JJA from March 2015 to October 2017. Low and high clouds are clearly separated, with a
290 band of minimum cloudiness in-between (near 4km Above Sea Level or ASL). Above both
291 surfaces CATS data show large amounts of high clouds during nighttime that get thinner
292 near noon as their base rise. The vertical evolution in the fraction of sampled atmosphere
293 due to attenuation by atmospheric components, for these diurnal cycles and all that follow,
294 is documented in Appendix C.

295 Significant differences exist between the cloud profiles diurnal cycle above land and ocean.
296 Clouds generally extend higher over land during nighttime: high clouds are vertically most
297 frequent near 10km over ocean, while they extend up to 14km above continents until 5AM.
298 Over ocean, high clouds appear to rise late in the afternoon (3-6PM) and fall soon thereafter
299 as night falls. Land-ocean differences are most striking at low altitudes: over Ocean low
300 clouds are present almost all day long between 0 and 2km ASL, their CF decreasing from a
301 20% maximum near 4AM to ~10% between 11AM and 5PM. Over land, low clouds are only
302 significant during daytime: they appear near 2km ASL at 10AM and extends upwards to
303 reach 4km ASL near 4PM. The associated CF remains low, at most 8%. These planetary
304 boundary layer (PBL) clouds are most certainly associated with turbulence and convection
305 activity occurring near the surface. They disappear after 4PM without connecting to the
306 higher layers. The clear-sky band (CF < 2%) near the surface is thickest at night (almost 2km)
307 and thinnest in the late morning.

308 An aside on cloud detection: over the ocean, CATS detects both low and high clouds more
309 frequently during nighttime. This suggests that the high clouds are optically thin enough for
310 letting CATS document the increase of lower clouds. If the reverse was true, more high
311 clouds would be systematically linked to fewer low clouds, which is not what we observe.
312 The frequency of high-level clouds observed in daytime could however be affected by the
313 decrease in cloud detection sensitivity due to solar pollution affecting the signal to noise



314 ratio. While CATS is seeing the diurnal cycle of high and low clouds, the magnitude of the
315 daytime cloud fractions could then be biased slightly low due to solar pollution and, at low
316 altitudes, cloud-aerosol discrimination issues.

317 While these seasonal mean results are informative, they mix together unrelated cloud
318 populations from hemispheres with opposite seasons driven by different circulation
319 regimes. We thus describe the daily cycles of clouds in zonal bands in the next section.

320



321 **3.2. Diurnal Cloud fraction profiles observed over mid-latitudes and Tropics**

322 In this section we consider cloud populations over four latitude bands: midlatitude (30°-51°
323 and Tropics (0-30°), in the North Hemisphere (NH) and South Hemisphere (SH), over land
324 and ocean. We first examine the differences between the diurnal cycles affecting the cloud
325 vertical profiles over ocean and land in JJA (Sect. 3.2.a and 3.2.b, Fig. 2), then we discuss
326 how these cycles are affected by the season by considering DJF results (Sect. 3.2.c, Fig. 3).

327

328 *a) High clouds*

329 As expected, Fig. 2 shows that high clouds are located at higher altitude in the tropics (12-
330 16km ASL) than in midlatitude (8-12km), following the variation of the troposphere depth
331 with latitude. Also as expected, the occurrence of high clouds is largest (CF > 20%) in deep
332 convection along the Inter Tropical Convergence Zone (ITCZ), located between 0° and 30°N
333 in JJA, and minimum (CF < 8%) in the subsidence branch of the Hadley cell (0°-30°S in JJA). In
334 mid-latitudes, high clouds (7-9km ASL) are far more frequent (CF ~ 20%) over the Southern
335 Ocean (30°S-51°S) than over the northern ocean (30-51°N).

336 Oceanic high clouds CF exhibits a marked maximum at nighttime and a pronounced
337 minimum at midday in all latitude ranges (tropics and mid latitudes). Even if this strong
338 diurnal cycle occurs at all latitudes (even in subsidence region), it is more pronounced where
339 the high clouds are more numerous: along the ITCZ (0-30°N) and in the Southern Ocean (30-
340 51°S). In addition to the variation in the high cloud occurrence, the vertical extent of these
341 clouds shows a marked diurnal cycle as well along the ITCZ: more than 4km near midnight,
342 less than 1km at noon. This thickening takes a few hours (5-10PM), while the morning
343 thinning is much sharper. By comparison, over the Southern Ocean the thickness of high
344 clouds remains quite stable throughout the day.

345 Overall, high clouds behave very similar above land (Fig. 2, right column) and ocean (Fig. 2,
346 left column) at all latitudes, except between 30-51°S where land surface is too small to
347 conclude.

348

349 *b) Low clouds*



350 Over ocean in JJA (Fig. 2), the occurrence of low clouds (0-3km ASL) changes significantly
351 with latitude: The Southern Ocean region (30-51°S) is by far the cloudiest, the mid-latitude
352 north (30-51°N) and the subsidence tropics (0-30°S) are moderately cloudy, and even less
353 low clouds are observed along the ITCZ (0-30°N). The oceanic low clouds show only small
354 variations along the day. A weak diurnal cycle occurs at all latitudes except along the ITCZ
355 (possibly because there the low clouds are in part masked by higher clouds affected by an
356 out-of-phase diurnal cycle). Low-level clouds are more numerous in nighttime (CF near 20%)
357 compared to daytime (CF~12%) in subsidence tropics (0-30°S) and mid-latitude north (30-
358 51°N). The southern oceanic low clouds exhibit a very faint diurnal cycle: their CF gets over
359 20% nearly all day long, with a very small decrease near 2PM.

360 In contrast to high clouds, the differences between land and ocean are striking for the low
361 and mid-level clouds. Both the occurrences and the diurnal cycles of clouds over land differ
362 significantly from their oceanic counterparts. The low clouds are very few over land (CF~4%)
363 compared to over ocean (>16%), all day long. Moreover, the continental low cloud diurnal
364 cycle exhibits a maximum in the early afternoon (around 2PM) that does not show up over
365 ocean: a maximum CF appears around 2.5 km of altitude in the upper edge (or just above
366 the top) of the atmospheric boundary layer; it is linked to convective activity between 10AM
367 and 5PM.

368 Another noticeable difference between land and ocean is the presence of well-defined mid-
369 level cloud population over NH tropical land (0-30°N, 2nd row on the right in Fig. 2) in the
370 free troposphere between 5 and 7 km ASL. These mid-level clouds show a diurnal cycle
371 opposite to PBL clouds and similar to the high clouds in that its minimum occurs at midday
372 and its maximum at night, although the magnitude of this cycle is much more limited.
373 Bourgeois et al. (2017) discussed similar clouds observed over West Africa: they found these
374 clouds reach maximum occurrence early in the morning, which is consistent with our results.

375

376 *c) Seasonal differences*

377 Figure 3 presents diurnal cycles of cloud fraction profiles over the same latitude bands as
378 Fig. 2 but based on data collected during the boreal winter (DJF). As seasons switch
379 hemispheres, we anticipate cloud populations to undergo symmetric changes across



380 hemispheres, in agreement with large-scale dynamic processes driving their spatial
381 distribution on seasonal time scales. This is verified for high clouds (Fig. 2 vs. Fig. 3): in the
382 Tropics the ITCZ moves to South and with it the large CF at high altitudes, in midlatitudes the
383 high clouds are more frequent during the winter season, due to more frequent low-pressure
384 conditions.

385 Interestingly, the mid-altitude clouds visible near 6km ASL in the NH Tropics over land (Fig. 2,
386 2nd row on the right) also move to the SH Tropics in DJF (Fig. 3, 3rd row on the right). This
387 confirms the year-long persistence of midlevel clouds over continental tropical regions found
388 by Bourgeois et al. (2017).

389 The seasonal changes in low clouds are less symmetric than in higher clouds, as they are
390 more closely related to surface conditions. Over ocean, in DJF the amount of low clouds
391 increases dramatically in NH midlatitudes compared to JJA (Fig. 2 and 3, top left), but does
392 not change noticeably in the SH midlatitudes: the diurnal cycle that sees a slight decrease in
393 the huge population of low clouds over the Southern Ocean is present in both seasons (Fig.
394 2 and 3, bottom left). Over land, in the Tropics, low clouds appear similar in frequency and
395 behaviour in both DJF and JJA: PBL clouds extend vertically between ~7AM to 5PM (Fig. 2
396 and 3, rows 2 and 3 of right column). The NH midlatitudes show the strongest seasonal
397 change in low clouds, as they become present all day long: the diurnal cycle associated with
398 PBL development in JJA disappears in DJF (Fig. 2 and 3, top right). SH midlatitude retrievals
399 over land are as noisy in DJF and JJA, but the DJF data (Fig. 3, bottom right) suggests that low
400 clouds there extend vertically a lot more than in JJA, up to 4km ASL.



401 **3.3. Diurnal cycle of cloud profiles above selected continental regions**

402

403 In this section, our first goal is to compare the diurnal cycle of the cloud fraction profiles
404 from CATS against independent observations collected by active instruments from ground-
405 based sites (Sect. 3.3.a and 3.3.b). In particular, we want to understand if the results shown
406 so far (Fig. 1-3) are valid for low clouds despite the attenuation of the space laser signal
407 (Sect. 2.2.a). Our second goal is to compare, for the first time, the diurnal cycle of the cloud
408 fraction profiles over different continental regions all over the globe as observed with a
409 single instrument (Sect. 3.3.c).

410

411 ***a) Over South of Paris in Europe***

412 Figure 4 shows the diurnal evolution of CF profiles seen by the ground-based LNA lidar (Fig.
413 4a) operated on the SIRTA site south of Paris (Sect. 2.1.b) and seen by CATS space lidar in a
414 10°x10° box centered on the same site, keeping only profiles sampled over land (Fig. 4b).
415 Both datasets report a well-defined high-altitude layer, with a clear-cut cloud top near 12
416 km ASL that rises up a few hundred meters in the morning until 10AM and slowly falls
417 during the afternoon by at most 1 km. In both figures the bottom of this layer is not sharply
418 defined: the CF decreases almost linearly from 20% near 11-12km ASL to near-zero at 4km
419 ASL. Both instruments also report a low-level cloud layer that extends upwards from ~1km
420 ASL at 5AM to ~4km ASL near 8PM.

421 Regarding differences, the space lidar sees a late-afternoon resurgence of high-altitude
422 clouds (starting near 5PM) absent from the ground-based lidar record. The space lidar also
423 reports a much lower frequency of boundary layer clouds: less than 10% throughout the
424 day. This difference gets particularly large in the late afternoon, when the ground-based
425 lidar reports the low-level CF rising above 20%. The large quantity of high-altitude clouds
426 observed by CATS at that time could impair its ability to detect lower clouds, while at the
427 same time the large quantity of low clouds observed by the ground lidar can impair its
428 ability to detect high clouds. The absence of precipitating clouds from the LNA dataset could
429 also explain this difference.

430 As expected, the spaceborne CATS lidar sees more high-level clouds and less low-level



431 clouds than the ground-based LNA lidar . This sampling bias affects all ground-space lidar
432 comparisons (e.g. Dupont et al., 2010). Even so, the diurnal cycle of the cloud altitudes are
433 roughly consistent from space and ground lidars. This comparison suggests the main
434 limitation of CATS is the capability to document the increase in low cloud occurrence in the
435 late afternoon.

436

437 ***b) Over the US Southern Great Plains ARM site***

438 Figure 4c shows the diurnal evolution of CF profiles based on CATS measurements in a
439 $10^{\circ}\times 10^{\circ}$ lat-lon box centered on the ARM SGP site (Sect. 2.2.b), keeping only profiles
440 sampled over land. High-level clouds near 12km Above Sea Level (ASL) are frequent during
441 nighttime, with large CF (above 20%) between 16:00 and 03:00 LT. The high cloud layers
442 also get thick and extend vertically between 9 and 14km ASL. The importance of high-level
443 clouds strongly drops during daytime (7AM-5PM), with CF dropping below 10% at midday.
444 The associated cloud layer gets much thinner, limiting its extent between 11 and 12km ASL
445 at its thinnest point (near 10AM). There are slightly more midlevel clouds (4-8km ASL) in the
446 early morning, with CF increasing to $\sim 10\%$ between midnight and 7AM. Midlevel clouds are
447 almost non-existent the rest of the day. PBL clouds form near the surface at 9AM, rise and
448 thicken almost up to 4km ASL near 4PM.

449 Most of these features derived from CATS observations are consistent with those derived
450 from summer observations by the ground-based MMCR (Fig. 3a, top left in Zhao et al., 2017)
451 and RL (Fig. 3, bottom right in Dupont et al., 2011 -- mind the x-axis in UTC, which brings the
452 local noon at 18UTC). For instance, Both CATS and the ground-based datasets report a
453 rather strong diurnal cycle of high clouds, which can be explained by possible influence from
454 Tropical dynamics at the 36°N latitude of the SGP site. There are some differences: both
455 MMCR and RL report a minimum in the high-level clouds near 5PM. The MMCR reports a
456 thinner extent of boundary layer clouds (up to 2.5km at most), while findings from the RL
457 are more consistent with those from CATS. The MMCR reports almost no low-level clouds
458 between 6PM and 6AM, while CATS and the RL report some clouds in that time frame --
459 they might be optically thin and missed by the radar. The RL reports almost none of the
460 daytime PBL clouds so conspicuous in MMCR and CATS observations, perhaps because fully
461 attenuating clouds were removed from the RL dataset for the Dupont et al. (2011) study as



462 they hide most of the atmosphere from a ground-based lidar (unlike a spaceborne one).

463 These deviations appear acceptable to us given the much smaller size of the CATS
464 dataset (infrequent overpasses over 3 seasons) compared to the daily local measurements
465 included in the MMCR and RL datasets (14 and 10 seasons). It is reassuring to find that CATS
466 results retain the major features of the clouds profile daily cycle. Most notably, CATS
467 provides a correct representation of the diurnal evolution of the altitude of low-level
468 boundary layer clouds (not the occurrence in late afternoon) despite the presence of high-
469 level clouds.

470 In this section we have seen that using retrievals from ground-based instruments as a
471 reference, CATS measurements seem to provide an interesting documentation of the clouds
472 diurnal cycle. Due to the distribution of ground-based sites, however, this validation
473 approach is limited to certain regions: mostly midlatitudes from the Northern Hemisphere.

474

475 ***c) Diurnal cycles of the cloud profiles over continents***

476 Continents are diverse in ground type, orography, latitude, exposition to large scale
477 atmospheric circulation, and transport of air masses from the local environment. These
478 factors influence the atmosphere above the continent, leading to possible variations in the
479 cloud diurnal cycle profiles. Ground-based observations let us document these different
480 cycles, but differences between instruments and operations in the different ground sites
481 make comparing diurnal cycle observed from ground at different locations difficult. Thanks
482 to CATS data, for the first time we compare here the cloud diurnal cycle profiles observed
483 over different continents by a single instrument and with a relatively large space sampling,
484 compared to single-site ground-based observations. Figure 5 illustrates how the diurnal
485 cycle of CF varies among seven large continental areas across both hemispheres, considering
486 only cloud detections made by CATS over land within lat-lon boxes (defined in the inset map)
487 during the summer seasons (JJA in the NH, DJF in the SH).

488 During summer most continents share a development of PBL clouds during sunlit hours
489 (with similar Cloud Fractions, hours and vertical extents), except NH Africa where low clouds
490 are almost absent. Most continents also share a nighttime maximum and daytime maximum
491 of high clouds, with an associated thinning during morning and thickening during the



492 afternoon. Variations in cloudiness and cloud thickness are particularly intense over South
493 America and SH Africa, while they are minimal over Australia. A mid-altitude cloud layer is
494 present almost all day long, with a faint daytime minimum, over all SH continents and NH
495 Africa.

496 Note that the present comparison is less robust in the lower troposphere than higher in the
497 troposphere, due to the attenuation of the space lidar signal as it penetrates the
498 atmosphere.

499



500 **4. Discussion**

501

502 Hereafter we use our results for answering the following questions: How does the diurnal
503 cycle of low, mid, high cloud covers from geostationary satellites compare with CATS ones?
504 Do the existing lidar space missions document extreme or average behaviours of the cloud
505 profile diurnal cycle? What about upcoming sun-synchronous lidar space missions?

506

507 **4.1 About the Diurnal cycles of Low and High Cloud Amounts**

508

509 CATS observations provide a first opportunity to compare the cloud diurnal cycle derived
510 from the ISCCP dataset (Sect. 2.1.c) with completely independent observations at near-
511 global scale (excluding latitudes higher than 51°). In particular, we expect an active sensor
512 technique (CATS) to be independent of the surface, contrarily to the passive remote sensing
513 observations (ISCCP) that may sometimes confound clouds and surface over reflective
514 surfaces such as ice and deserts. Moreover, CATS is expected to observe more optically thin
515 clouds than passive sensors thanks to a lidar high sensitivity. Since CATS sampling is
516 constrained between 51°S and 51°N, its data cannot be used to document the diurnal cycle
517 in the polar regions, like ISCCP does: our comparison will extend at most to midlatitudes.

518 Figure 6 shows the diurnal cycle of the Low and High cloud covers observed by the CATS
519 space lidar, plotted in a similar way as Figure 11 in RS99 for easier comparison.

520 Over ocean CAs are very stable, the diurnal cycle is almost flat (Fig. 6, left column). CATS
521 shows a weak cycle for low clouds, with a maximum in mid-morning and a minimum in
522 early-afternoon, which is also visible in ISCCP data. For oceanic high clouds, CATS exhibit
523 almost no diurnal cycle except in the Tropics where they follow the same cycle as low
524 clouds. ISCCP also shows a weak cycle for high clouds, but opposite to the CATS one. This
525 might be related to the fact that CATS can detect optically thin high clouds better than
526 ISCCP. The optically thicker high clouds seen by ISCCP are thus probably more linked to deep
527 convection activity. CATS can better detect optical thin high clouds, which should be more
528 decoupled from convection and less affected by diurnal cycles.

529 Over land, between 15°S and 60°N, CATS reports that low-clouds have a pronounced diurnal



530 cycle with a maximum of low-level clouds at midday (+10%) and a minimum at midnight (-
531 5%). This is consistent with ISCCP observations (Figure 11 in RS99), but in the Northern mid-
532 latitudes the amplitude of the cycle is weaker for CATS than ISCCP (minimum at -4% instead
533 of -12%). For high-level clouds over land in the Tropics (15°S-30°N) CATS observes a
534 maximum during night-time and a minimum at noon; the timing is consistent with ISCCP but
535 the amplitude is slightly more pronounced with CATS than ISCCP (-12% instead of -7% at
536 midday). In the Southern hemisphere (15°S-60°S) the similarity between CATS and ISCCP
537 gets lost, probably because the land surface is small in those latitude ranges and the
538 observations are not significant.

539 In summary CATS confirms the shape of the Low and High cloud diurnal cycles observed by
540 ISCCP except for high tropical clouds, likely because the space lidar can detect more
541 optically thinner clouds that are not directly linked to deep convection. In most cases, the
542 amplitudes of the diurnal cycle observed by CATS differ from those observed by ISCCP.

543 Both CATS and ISCCP miss some low clouds that are masked by the presence of high thick
544 clouds. So even if CATS and ISCCP diurnal cycle are roughly consistent in low clouds, both
545 results might be biased in the same direction. The high clouds diurnal cycle presented here
546 are more robust than the low clouds ones.

547

548 **4.2 About the Cloud Fraction profiles observed at fixed local times by space lidars**

549 The CALIOP lidar has provided detailed Cloud Fraction profiles since 2006 at 0130AM and
550 0130 PM LT. The next spaceborne atmospheric lidar missions ADM-Aeolus, to be launched
551 in late 2018 (Culoma et al., 2017) on a sun-synchronous orbit, will enable measurements at
552 0600AM and 0600PM LT. After that, the ATLID lidar on the Earth-CARE platform (Illingworth
553 et al., 2015), expected to launch in 2020, will operate at fixed local times close to CALIOP
554 (02:00AM and PM). The CATS dataset may remain for the near future our single source of
555 diurnally distributed cloud profile lidar measurements from space.

556

557 *a) Comparison between CATS and CALIPSO*

558 In this section we first check how CATS sees the day/night variation in cloud profiles also



559 documented by CALIOP through its two daily overpasses. Figure 7 shows vertical profiles of
560 Cloud Fraction reported by both datasets at 0130AM and PM, over ocean (left) and land
561 (right), latitude-weighted and averaged between 51°S and 51°N over JJA between 2015 and
562 2017. The black lines show the CF obtained when considering all measurements from both
563 instruments. Over land and ocean, we find that both CALIPSO and CATS overall report larger
564 Cloud Fractions at 0130AM (blue) than 0130PM (red), in agreement with the findings of
565 Gupta et al. (2018). Below 2.5 km, this difference is stronger over ocean (+7% in 0130AM
566 CF) than over land. Both datasets report a strong increase in 0130AM CF (almost +7%
567 compared to 0130PM) above 15km over land.

568 The CF profiles reported by both datasets agree very well over Ocean (left) in both daytime
569 and nighttime conditions. Over land (right) in daytime (red) conditions, CATS reports slightly
570 more low-level clouds (CF~7% near 1km ASL, ~5% for CALIOP). This difference, which is
571 present at all latitudes above land during daytime (not shown), might be due to the so-
572 called single-shot low clouds, for which CALIOP data undergoes a specific processing
573 (Winker et al., 2009). The strongest differences appear for nighttime CF over land (right,
574 blue): CALIPSO CF is larger than CATS CF by a 2-3% throughout the entire profile. A perfect
575 agreement between CF from both datasets should not be expected, as the CATS and CALIOP
576 lidars operate in different configurations – wavelengths, pulse repetition frequencies and
577 signal-to-noise ratios are different, for a start. These technical variations lead to differences
578 in, for instance, how fast the laser pulse energy of both instruments gets attenuated as it
579 penetrates atmospheres of various compositions, or differences in cloud detection
580 performance, e.g. when sampling optically thin clouds in the upper troposphere, or
581 fractionated boundary layer clouds (see Reverdy et al., 2015 for a study of the impact of
582 design choices on lidar retrievals). Both datasets agree quite well on the general vertical
583 pattern of the profile, though. A useful conclusion is that considering CALIPSO observations
584 at both overpass local times (i.e. 0130AM and 0130PM) apparently provides a good
585 approximation of the daily average Cloud Fraction profile.

586

587 b) Comparison of cloud fraction profiles at various times of satellite overpass

588 As a final analysis, we represent the range covered by CATS hourly Cloud Fraction profiles
589 over a day (averaged over the globe - white envelope in Fig. 8) and show CF profiles



590 observed by CATS ± 1 hour around the fixed local observation times of the three sun-
591 synchronous space lidar missions (CALIPSO, ADM-Aeolus, EarthCare).

592 Our first aim is to understand how wind observations made at fixed local time by ADM-
593 Aeolus might be impacted by the cloud diurnal cycle. ADM-Aeolus will provide information
594 on wind only in absence of clouds. Figure 8 indicates that ADM-Aeolus overpass times are
595 quite cloudy in both AM and PM compared to the diurnal variability (white envelope). The
596 PM overpass corresponds to daily maximum in cloud profiles over both ocean and land,
597 while AM observations correspond to a time representative of the daily average cloud
598 fraction profile. As more clouds occur in the PM than AM observations, less wind
599 information will likely be provided by ADM-Aeolus in the afternoon than in the morning. For
600 the future, another ADM-Aeolus-like mission around midday (minimum cloud fraction
601 profile) would increase the number of wind measurement with respect to the cloud
602 occurrence.

603 Our second aim is to understand how well observations made at fixed local times by space
604 lidar dedicated to clouds studies (CALIPSO and EarthCare) capture the daily variability of
605 cloud fraction profiles. Figure 8 suggests that over land (right), CALIPSO and Earth-CARE
606 retrievals capture only part of the daily CF variability above 8km ASL: the PM measurements
607 overestimate the daily CF minima and the AM measurements underestimate the daily CF
608 maxima. Below 8km ASL they are rather representative of the daily average, except below
609 5km ASL where PM measurements get close to the daily CF maxima. Figure 8 also shows
610 that over Ocean (left) CALIPSO and Earth-CARE retrievals should be considered as the daily
611 CF maxima during the nighttime (AM) overpass and as the daily CF minima during the
612 daytime (PM) overpass. This has interesting implications: it suggests that not only CALIPSO
613 but all the observations dedicated to cloud studies collected by the instruments within the
614 A-train (CloudSat, CERES, MODIS, PARASOL, etc.) have documented the state of the
615 atmosphere in the extreme states of the cloud profile diurnal cycle over the last 12 years
616 over ocean. These conclusions suggest the A-Train observations are likely relevant and
617 robust to constrain the cloud diurnal cycle extremes in climate models and climate studies.

618

619



620

621

622 **5. Conclusions**

623 In this paper we took advantage of the variable local time of overpass of the International
624 Space Station to document the diurnal cycle of the cloud vertical profile as seen by the CATS
625 lidar. This is the first time the diurnal evolution of the vertical cloud profile is documented on
626 that vertical scale on a large part of the globe, between 51°S and 51°N. Our results are based
627 on 15 months of systematic observations (3 boreal summers and 2 austral summers)
628 collected during the 2015-2017 time period, which enable statistically significant results.

629 The main results are the following. We observed the high tropical clouds start getting thicker
630 late in the afternoon (4-5PM) and reach their maximum thickness of 4-5km near 10PM. This
631 thickening is particularly intense in the Summer Hemisphere in DJF. Our results reveal a mid-
632 level cloud layer (4-8 km ASL) persistent all day long over the tropical continent during
633 summer, with a weak diurnal cycle (minimum at noon). Southern Ocean results are quite
634 unique; this ocean is covered by low clouds (0-2km ASL) all day long in summer and winter. A
635 slight diurnal cycle sees their CF drop by a few percents during the afternoon (from noon to
636 6PM), but their thickness stays constant. High clouds are also frequent over the Southern
637 Ocean, more so in JJA, and follow all year long an earlier diurnal cycle, with an early morning
638 to early afternoon minimum (from 8AM and 3PM). At all latitudes, continental low clouds
639 are most frequent in the early afternoon (around 2PM) at about 2.5 km ASL. Our results also
640 show that the diurnal cycle of clouds in summer share similar features over continents in
641 both hemispheres: the rapid development of near-surface clouds during sunlit hours and an
642 increase in cloudiness and cloud thickness at high altitudes during nighttime (stronger over
643 the SH and the Tropics). Exceptions are NH Africa, where PBL clouds are very rare, and
644 Australia, where high clouds appear only significant between 8 and 11PM.

645 We evaluated the diurnal cycle derived from CATS against independent ground-based
646 observations and found satisfactory agreement. Moreover, we discussed the implications of
647 our results for spaceborne instruments from sun-synchronous satellite missions (CALIPSO
648 and the A-train, ADM, Earth-CARE). Our results suggest that cloud profiles from CALIPSO and
649 Earth-CARE over oceans should nearly describe the daily minimum of the cloud fraction



650 vertical profile during their PM overpass, and its daily maximum during their AM overpass,
651 which supports the idea that all data collected by A-train instruments (not only CALIPSO)
652 are very relevant to document the cloud diurnal cycle. This is also roughly the case over land
653 at altitudes above 8km ASL, although the amplitude of the diurnal variability is quite
654 underestimated.

655 In the future, it would be possible to consider CATS measurements at smaller scales, to
656 identify regionally consistent cloud populations and diurnal behaviors over specific regions
657 of interest. It would also be possible to use CATS detection of opaque cloud layers to identify
658 the best local time of observation from space to study local cloud radiative effects. We hope
659 to address these lines of research in upcoming papers.

660 **Acknowledgments**

661 CALIPSO and CloudSat datasets were provided by the NASA Langley Research Atmospheric
662 Science Data Center (ASDC) and through the AERIS and ICARE/CGTD Data services. Data
663 were analyzed on the Climserv IPSL computing facilities. This research was made possible
664 through support by CNRS. We want to thank J.-L. Baray and N. Montoux for useful
665 discussions.

666

667



668 **References**

669

- 670 • Ackerman, T. P., and G. M. Stokes (2003), The Atmospheric Radiation Measurement
671 Program Phys. Today, 56, 38–44, doi:10.1063/1.1554135
- 672 • Bouniol, D., R. Roca, T. Fiolleau, and D.E. Poan, 2016: [Macrophysical, Microphysical,
673 and Radiative Properties of Tropical Mesoscale Convective Systems over Their Life
674 Cycle](#). *J. Climate*, **29**, 3353–3371, doi:10.1175/JCLI-D-15-0551.1
- 675 • Bourgeois, E., D. Bouniol, F. Couvreur, F. Guichard, J. H. Marsham, L. Garcia-Carreras,
676 C. E. Birch, and D. J. Parker (2018), Characteristics of mid-level clouds over West
677 Africa, *QJRM*, **113**, D04210–17, doi:10.1002/qj.3215.
- 678 • Ceppi, P., F. Briant, M. D. Zelinka, and D. L. Hartmann, 2017: Cloud feedback
679 mechanisms and their representation in global climate models, *WIREs Climate
680 Change* 2017, e465. Doi: 10.1002/wcc.465
- 681 • Cesana, G., and H. Chepfer (2013), Evaluation of the cloud thermodynamic phase in a
682 climate model using CALIPSO-GOCCP, *J. Geophys. Res.*, **118**(14), 7922–7937,
683 doi:10.1002/jgrd.50376.
- 684 • Chiriaco M., S. Bastin, P. Yiou, M. Haeffelin, J.-C. Dupont, L. Klenov, M. Stéfanon,
685 2014: European heat-wave in July 2006: observations and modelling showing how
686 local processes amplify conducive large-scale conditions. *Geophys. Res. Let.*, **41** issue
687 **15**, 5644 – 5652.
- 688 • Chiriaco, M., Dupont, J.-C., Bastin, S., Badosa, J., Lopez, J., Haeffelin, M., Chepfer, H.,
689 and Guzman, R.: ReOBS: a new approach to synthesize long-term multi-variable
690 dataset and application to the SIRTAs supersite, *Earth Syst. Sci. Data Discuss.*,
691 <https://doi.org/10.5194/essd-2017-101>, in review.
- 692 • Culoma A., A. Elfving, R. Meynart, A. Straume, D. Wernham, "AEOLUS mission: the
693 latest preparations before launch", *Proc. SPIE 10423, Sensors, Systems, and Next-
694 Generation Satellites XXI*, 1042303 (29 September 2017); doi: 10.1117/12.2282159
- 695 • Dupont, J. C., M. Haeffelin, Y. Morille, V. Noel, P. Keckhut, D. Winker, J. Comstock, P.
696 Chervet, and A. Roblin (2010), Macrophysical and optical properties of midlatitude



- 697 cirrus clouds from four ground-based lidars and collocated CALIOP observations, *J.*
698 *Geophys. Res.*, 115(D4), D00H24–15, doi:10.1029/2009JD011943.
- 699 • Elouragini, S. and Flamant, P. H.: Iterative method to determine an averaged lidar
700 ratio and the range resolved extinction in cirrus, *Appl. Opt.*, 35, 1512–1518, 1996.
- 701 • Guzman, R., H. Chepfer, V. Noel, T. Vaillant de Guélis, J. E. Kay, P. Raberanto, G.
702 Cesana, M. A. Vaughan, and D. M. Winker (2017), Direct atmosphere opacity
703 observations from CALIPSO provide new constraints on cloud-radiation interactions,
704 *J. Geophys. Res.*, 1–20, doi:10.1002/2016JD025946.
- 705 • Haeffelin, M. et al. (2005), SIRTa, a ground-based atmospheric observatory for cloud
706 and aerosol research, *Annales Geophysicae*, 23(2), 253–275, doi:10.5194/angeo-23-
707 253-2005.
- 708 • Haynes, J. M., T. H. Vonder Haar, T. L'Ecuyer and D. Henderson (2013) Radiative
709 heating characteristics of earth's cloudy atmosphere from vertically resolved active
710 sensors. *Geophys Res Lett* 40:624–904 630. doi:10.1002/grl.50145.
- 711 • Illingworth, A. J. et al. (2015), The EarthCARE Satellite: The Next Step Forward in
712 Global Measurements of Clouds, Aerosols, Precipitation, and Radiation, *Bull. Am.*
713 *Met. Soc.*, 96(8), 1311–1332, doi:10.1175/BAMS-D-12-00227.1.
- 714 • Kato, S., F. G. Rose, S. S. Mack, W. F. Miller, and co-authors (2011), Improvements of
715 top-of-atmosphere and surface irradiance computations with CALIPSO-, CloudSat-,
716 and MODIS-derived cloud and aerosol properties. *J Geophys Res* 116:D19209.
717 doi:10.1029/2011JD016050
- 718 • Konsta, D., J. L. Dufresne, H. Chepfer, A. Idelkadi, and G. Cesana (2016), Use of A-train
719 satellite observations (CALIPSO–PARASOL) to evaluate tropical cloud properties in the
720 LMDZ5 GCM, *Clim. Dyn.*, 1–22, doi:10.1007/s00382-015-2900-y.
- 721 • Kummerow, C., W. Barnes, T. Kozu, J. Shiue, and J. Simpson (1998), The Tropical
722 Rainfall Measuring Mission (TRMM) sensor package, *J. Atmos. Oceanic Technol.*, 15,
723 809–817.
- 724 • L'Ecuyer, T. S., N. B. Wood, T. Haladay, G. L. Stephens, and P. W. Stackhouse
725 Jr. (2008), Impact of clouds on atmospheric heating based on the R04 CloudSat fluxes



- 726 and heating rates data set, *J. Geophys. Res.*, 113, D00A15,
727 doi:[10.1029/2008JD009951](https://doi.org/10.1029/2008JD009951).
- 728 • L'Ecuyer, T. S., and J. H. Jiang, 2010: Touring the atmosphere aboard the A-Train.
729 *Physics Today*, vol .63 (7), 36-40.
- 730 • McGill, M. J., J. E. Yorks, V. S. Scott, A. W. Kupchock, and P. A. Selmer (2015), The
731 Cloud-Aerosol Transport System (CATS): A technology demonstration on the
732 International Space Station, *Proc. SPIE 9612, Lidar Remote Sensing for Environmental*
733 *Monitoring XV*, 96120A, doi:10.1117/12.2190841.
- 734 • Moran, K. P., B. E. Martner, M. J. Post, R. A. Kropfli, D. C. Welsh, and K. B. Widener
735 (1998), An unattended cloud-profiling radar for use in climate research, *Bull. Am.*
736 *Meteorol. Soc.*, 79, 443–455.
- 737 • Palm, S. P., D. L. Hlavka, P. Selmer, R. Pauly, 2016: the Cloud Aerosol Transport System
738 (CATS) Data Product Catalog release 3.0. Retrieved on January 23rd 2018 from
739 https://cats.gsfc.nasa.gov/media/docs/CATS_Data_Products_Catalog.pdf
- 740 • Pappalardo, G., Amodeo, A., Apituley, A., Comeron, A., Freudenthaler, V., Linné, H.,
741 Ansmann, A., Bösenberg, J., D'Amico, G., Mattis, I., Mona, L., Wandinger, U., Amiridis,
742 V., Alados-Arboledas, L., Nicolae, D., and Wiegner, M.: EARLINET: towards an
743 advanced sustainable European aerosol lidar network, *Atmos. Meas. Tech.*, 7, 2389-
744 2409, doi:10.5194/amt-7-2389-2014, 2014
- 745 • Reverdy, M., Noel, V., Chepfer, H., & Legras, B. (2012). On the origin of subvisible
746 cirrus clouds in the tropical upper troposphere. *Atmospheric Chemistry and Physics*,
747 12(24), 12081–12101. <http://doi.org/10.5194/acp-12-12081-2012>
- 748 • Reverdy, M., H. Chepfer, D. Donovan, V. Noel, G. Cesana, C. Hoareau, M. Chiriaco, and
749 S. Bastin (2015), An EarthCARE/ATLID simulator to evaluate cloud description in
750 climate models, *J. Geophys. Res.*, 120(2), 11, doi:10.1002/2015JD023919.
- 751 • Sèze, G., J. Pelon, M. Derrien, H. Le Gléau, and B. Six (2014), Evaluation against
752 CALIPSO lidar observations of the multi-geostationary cloud cover and type dataset
753 assembled in the framework of the Megha-Tropiques mission, *QJRMMS*, 141(688),
754 774–797, doi:10.1002/qj.2392.



- 755 • Soden, B. J. (2000), The diurnal cycle of convection, clouds, and water vapor in the
756 tropical upper troposphere. *Geophys. Res. Lett.* 27 (15), 2173-2176. doi:
757 10.1029/2000GL011436
- 758 • Stephens, G. L., & Kummerow, C. D. (2007). The Remote Sensing of Clouds and
759 Precipitation from Space: A Review. *Journal of the Atmospheric Sciences*, 64(11),
760 3742–3765. <http://doi.org/10.1175/2006JAS2375.1>
- 761 • Stephens, G., D. Winker, J. Pelon, C. Trepte, D. Vane, C. Yuhas, T. L'Ecuyer, and M.
762 Lebsack, 2017: CloudSat and CALIPSO within the A-Train: Ten years of actively
763 observing the Earth system. *Bull. Amer. Meteor. Soc.* doi:10.1175/BAMS-D-16-
764 0324.1, in press.
- 765 • Vaughan, M. A., K. A. Powell, D. M. Winker, C. A. Hostetler, R. E. Kuehn, W. H. Hunt, B.
766 J. Getzewich, S. A. Young, Z. Liu, and M. J. McGill (2009), Fully Automated Detection
767 of Cloud and Aerosol Layers in the CALIPSO Lidar Measurements, *J. Atmos. Oceanic*
768 *Technol.*, 26(10), 2034–2050, doi:10.1175/2009JTECHA1228.1.
- 769 • Winker, D., M. A. Vaughan, A. Omar, Y. Hu, and K. A. Powell (2009), Overview of the
770 CALIPSO mission and CALIOP data processing algorithms, *J. Atmos. Oceanic Technol.*,
771 26, 2310–2323.
- 772 • Winker DM, Pelon J, Coakley JA Jr, Ackerman SA, Charlson RJ, Colarco PR, Flamant P,
773 Fu Q, Hoff RM, Kittaka C, Kubar TL, Le Treut H, McCormick MP, Mégie G, Poole L,
774 Powell K, Trepte C, Vaughan MA, Wielicki BA. 2010. The CALIPSO mission: A global 3D
775 view of aerosols and clouds. *Bull. Am. Meteorol. Soc.* 91: 1211–1229.
- 776 • Winker, D., Chepfer, H., Noel, V. and X. Cai. : Observational Constraints on Cloud
777 Feedbacks: The Role of Active Satellite Sensors. *Surve in Geophys* (2017).
778 Doi:10.1007/s10712-017-9452-0
- 779 • Wylie, D. (2008), Diurnal Cycles of Clouds and How They Affect Polar-Orbiting
780 Satellite Data, *J. Climate*, 21(16), 3989–3996, doi:10.1175/2007JCLI2027.1.
- 781 • Yorks, J. E., M. J. McGill, S. P. Palm, D. L. Hlavka, P. A. Selmer, E. P. Nowotnick, M. A.
782 Vaughan, S. D. Rodier, and W. D. Hart (2016a), An overview of the CATS level 1
783 processing algorithms and data products, *Geophys. Res. Lett.*, 43, 4632–4639,



- 784 doi:[10.1002/2016GL068006](https://doi.org/10.1002/2016GL068006).
- 785 • Yorks, J. E., S. P. Palm, M. J. McGill, D. L. Hlavka, W. D. Hart, P. A. Selmer, E.
786 Nowotnick (2016b), CATS Algorithm Theoretical Basis Document, Level 1 and Level 2
787 Data Products, release 1.2. Retrieved on February 13th 2018 from
788 https://cats.gsfc.nasa.gov/media/docs/CATS_ATBD.pdf
- 789 • Yorks, J. E., S.D. Rodier, E. Nowotnick, P.A. Selmer, M.J. McGill, S.P. Palm, and M. A.
790 Vaughan (2018), CATS Level 2 Vertical Feature Mask Algorithms and Data Products:
791 An Overview and Initial Assessment, Atmos. Meas. Tech. Discuss., in preparation.
- 792 • Zhao, W., R. Marchand, and Q. Fu (2017), The diurnal cycle of clouds and
793 precipitation at the ARM SGP site: Cloud radar observations and simulations from the
794 multiscale modeling framework, J. Geophys. Res., 122(14), 7519–7536,
795 doi:[10.1002/2016JD026353](https://doi.org/10.1002/2016JD026353).



796 Figures.

797

798 Figure 1: (top) Map of the portion of the Earth sampled by CATS, in white: ~78% of the
799 Earth's surface. (bottom) Evolution of the vertical profile of Cloud Fraction as a function of
800 local time of observation over the Ocean (left) and Land (right), using CATS detections made
801 in JJA from 2015 to 2017.

802

803 Figure 2. Like Fig. 1, over the North Hemisphere midlatitudes (top row) and Tropics (second
804 row), the South Hemisphere Tropics (third row) and midlatitudes (bottom row) during JJA
805 from 2015 to 2017.

806

807 Figure 3: Same as Fig. 2, considering data CATS measured during the boreal winter (DJF,
808 from 2015 to 2017).

809

810 Figure 4: The diurnal cycle of clouds as seen (a) by the ground-based LNA lidar from its SIRTA
811 site in JJA during precipitation-free days over the 2003-2015 period, (b) by the space lidar
812 CATS in JJA 2015-2017 within a $10^{\circ} \times 10^{\circ}$ lat-lon box centered on SIRTA, considering only
813 sunlit conditions for consistency with LNA records, and (c) by the space lidar CATS in JJA
814 2015-2017 within a $10^{\circ} \times 10^{\circ}$ lat-lon box centered on the ARM SGP time. Time is local.

815

816 Figure 5: Diurnal cycle of the cloud fraction profiles observed by CATS over different
817 continents a) NH America, b) Europe, c) China, d) NH Africa, e) SH America, f) SH Africa, g)
818 Australia, averaged over the summer seasons (JJA in the North Hemisphere, DJF in the South
819 Hemisphere) from 2015 to 2017. For each region we considered all profiles sampled over
820 land within the boundaries shown by the inset map. CF over Europe do not extend as high
821 altitudes as the rest, as it is the only region that do not include part of the Tropical band.

822

823 Figure 6: Mean diurnal variations of low-level (solid line) and high-level (dotted line) cloud
824 amounts (%) every 3 hours in five zonal bands over ocean (left) and land (right) in JJA from
825 CATS for the period 2015-2017. Plots (a-f) are presented in a similar way as Figure 11 in RS99
826 for comparison.



827

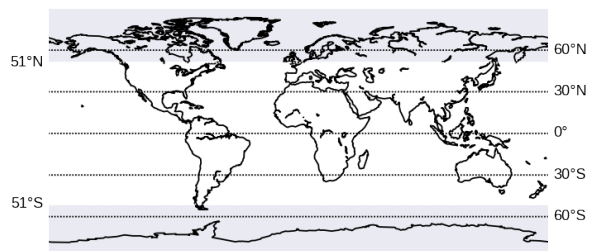
828 Figure 7: Vertical Profiles of Cloud Fraction observed by CALIPSO (full line) and CATS (dashed
829 line) between $\pm 51^\circ$ around 0130AM (blue), 0130PM (red) and at all times (black), over ocean
830 (left) and land (right). Measurements were weighted based on the latitude at which they
831 were made, to account for the different zonal sampling distributions of both instruments.
832 CALIOP cloud profiles were built using cloud layers from the CALIPSO v4.10 level 2, 5-km
833 cloud layer product. Only layers with a Cloud/Aerosol Discrimination score (CAD_Score)
834 above 0.7 were considered to build the CALIOP profiles, and layers with a
835 Feature_Type_Score above 5 were considered to build the CATS profiles. For both
836 instruments, we used JJA observations from 2015 to 2017.

837

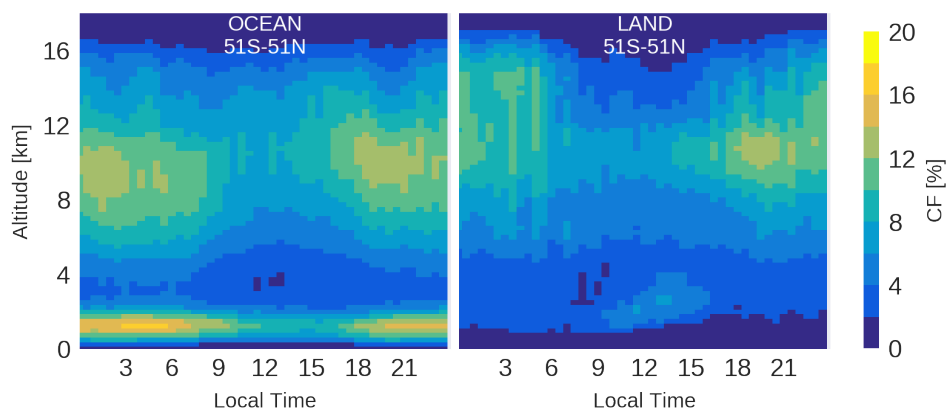
838 Figure 8: Mean Cloud fraction profiles observed by CATS at the overpass local time of the
839 sun-synchronous space lidars (CALIPSO and the A-train 01:30UTC, ADM 06:00UTC, Earth-
840 CARE 02:00UTC) compared to the envelope of the whole cloud fraction profile diurnal cycle
841 observed by CATS (white), averaged between $\pm 51^\circ$ over ocean (left) and land (right).
842 CALIPSO and Earth-CARE are dedicated to clouds and aerosols studies, while ADM is primarily
843 dedicated to wind measurements in non-cloudy conditions. We used CATS observations
844 during JJA from 2015 to 2017.

845

846

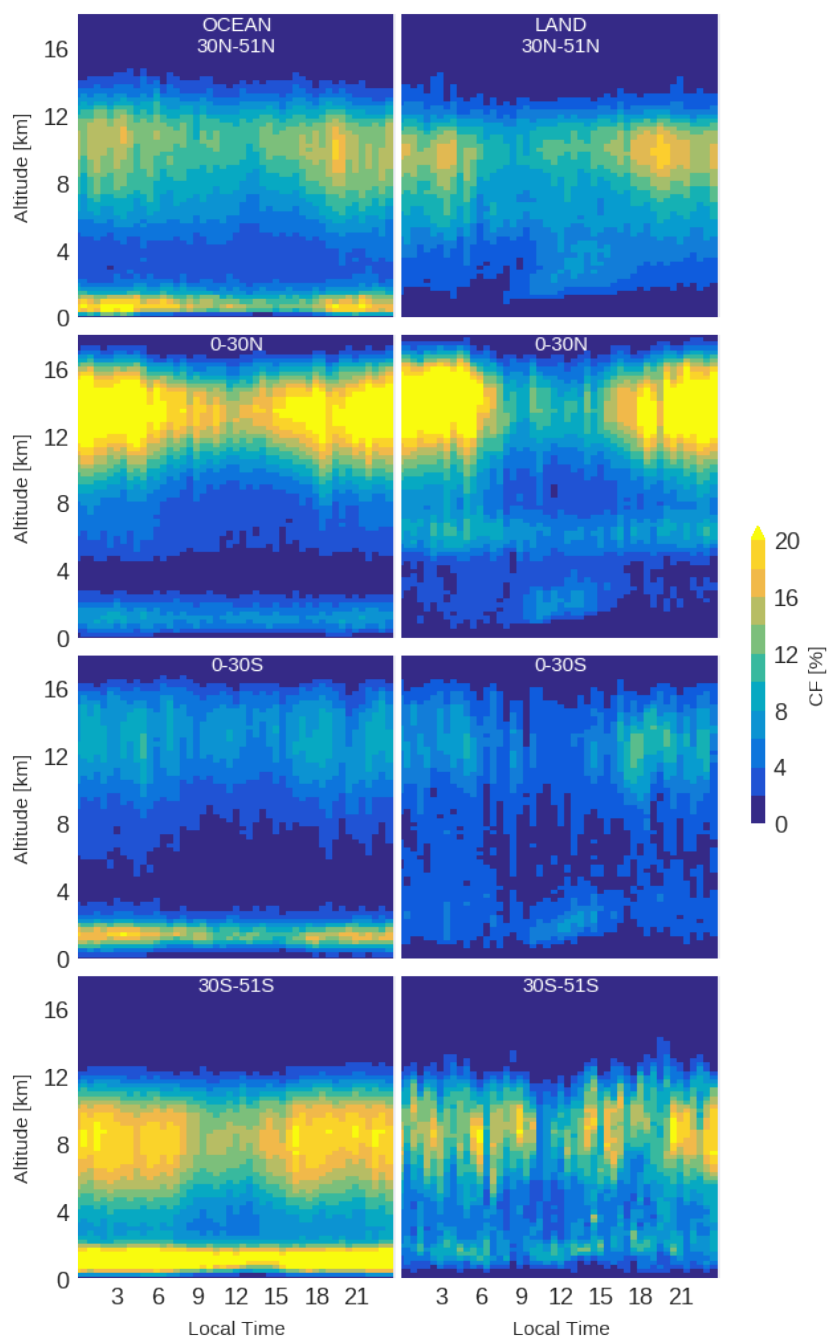


847



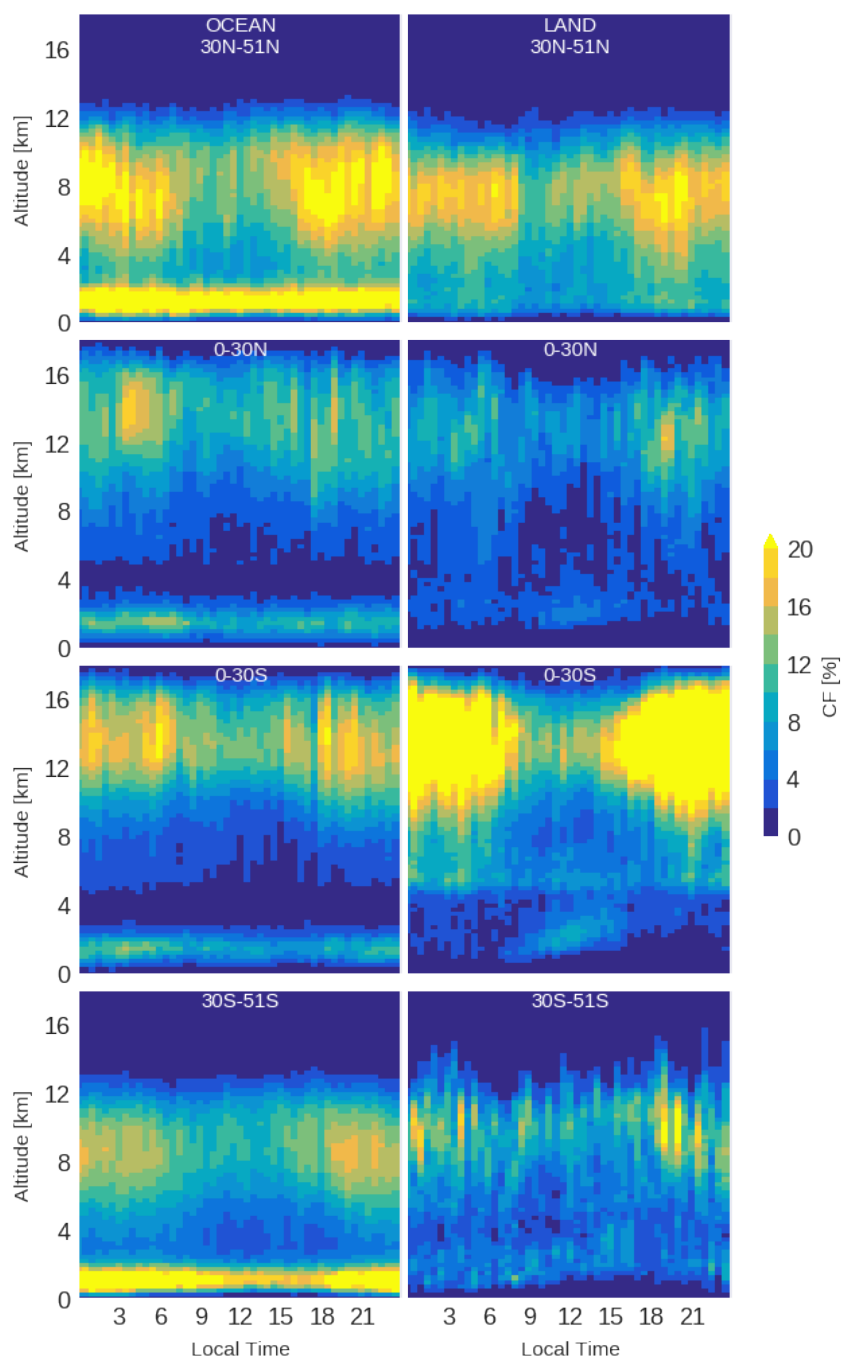
848

849 Figure 1: (top) Map of the portion of the Earth sampled by CATS, in white: ~78% of the
 850 Earth's surface. (bottom) Evolution of the vertical profile of Cloud Fraction as a function of
 851 local time of observation over the Ocean (left) and Land (right), using CATS detections made
 852 in JJA from 2015 to 2017.



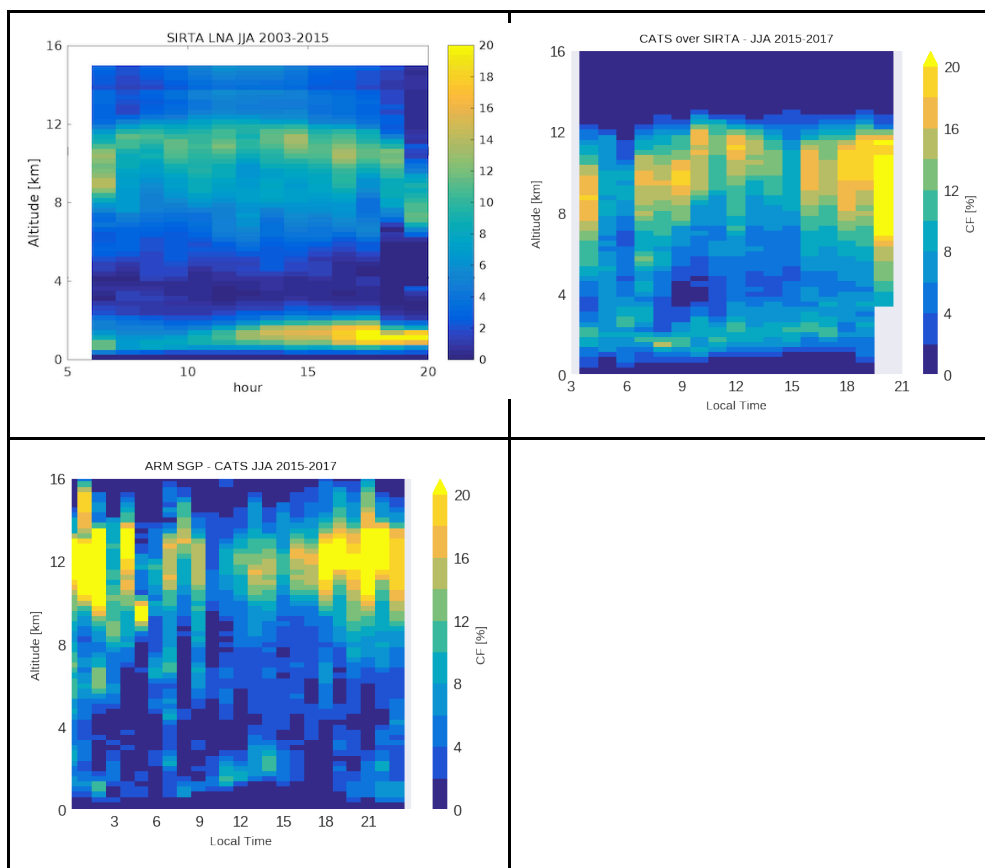
853

854 Figure 2. Like Fig. 1, over the North Hemisphere midlatitudes (top row) and Tropics (second
855 row), the South Hemisphere Tropics (third row) and midlatitudes (bottom row) during JJA
856 from 2015 to 2017.



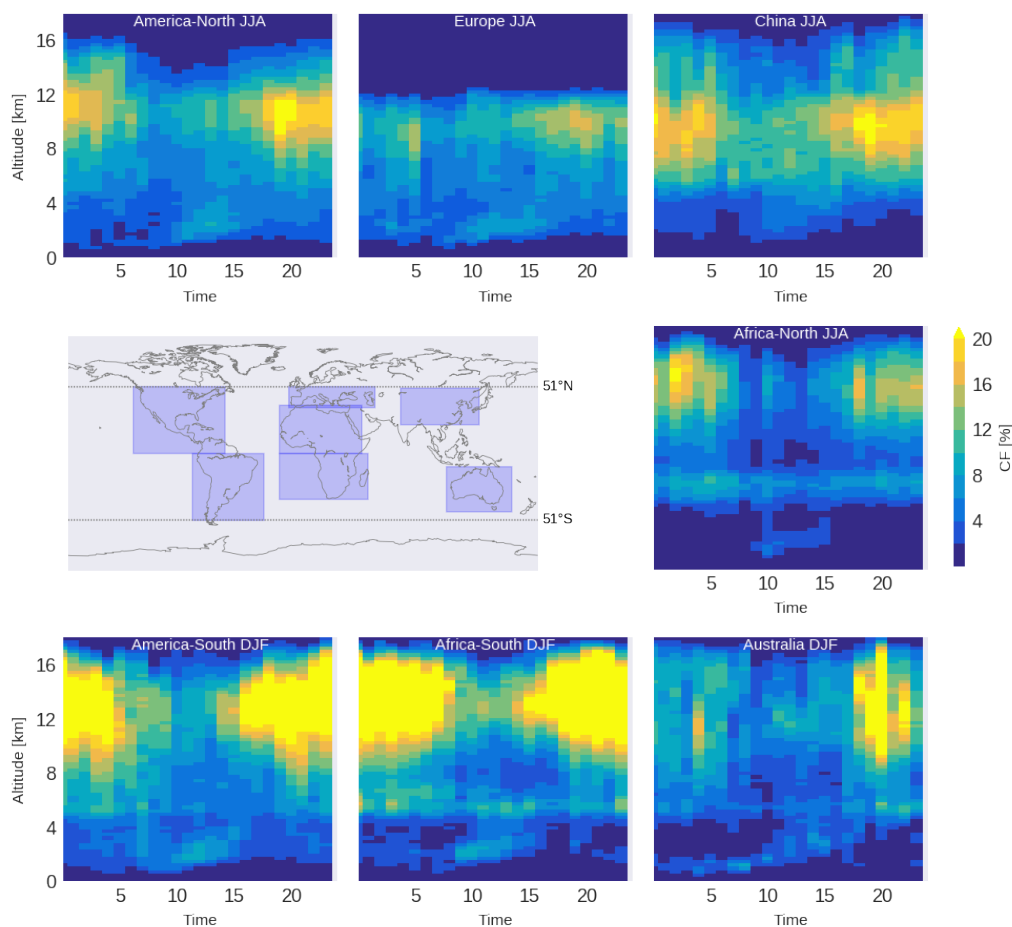
857

858 Figure 3: Same as Fig. 2, considering data CATS measured during the boreal winter (DJF,
859 from 2015 to 2017).



860

861 Figure 4: The diurnal cycle cloud profiles as seen (a) by the ground-based LNA lidar from its
862 SIRT A site in JJA during precipitation-free days over the 2003-2015 period, (b) by the space
863 lidar CATS in JJA 2015-2017 within a 10°x10° lat-lon box centered on SIRT A, considering only
864 sunlit conditions for consistency with LNA records, and (c) by the space lidar CATS in JJA
865 2015-2017 within a 10°x10° lat-lon box centered on the ARM SGP time. Time is local.

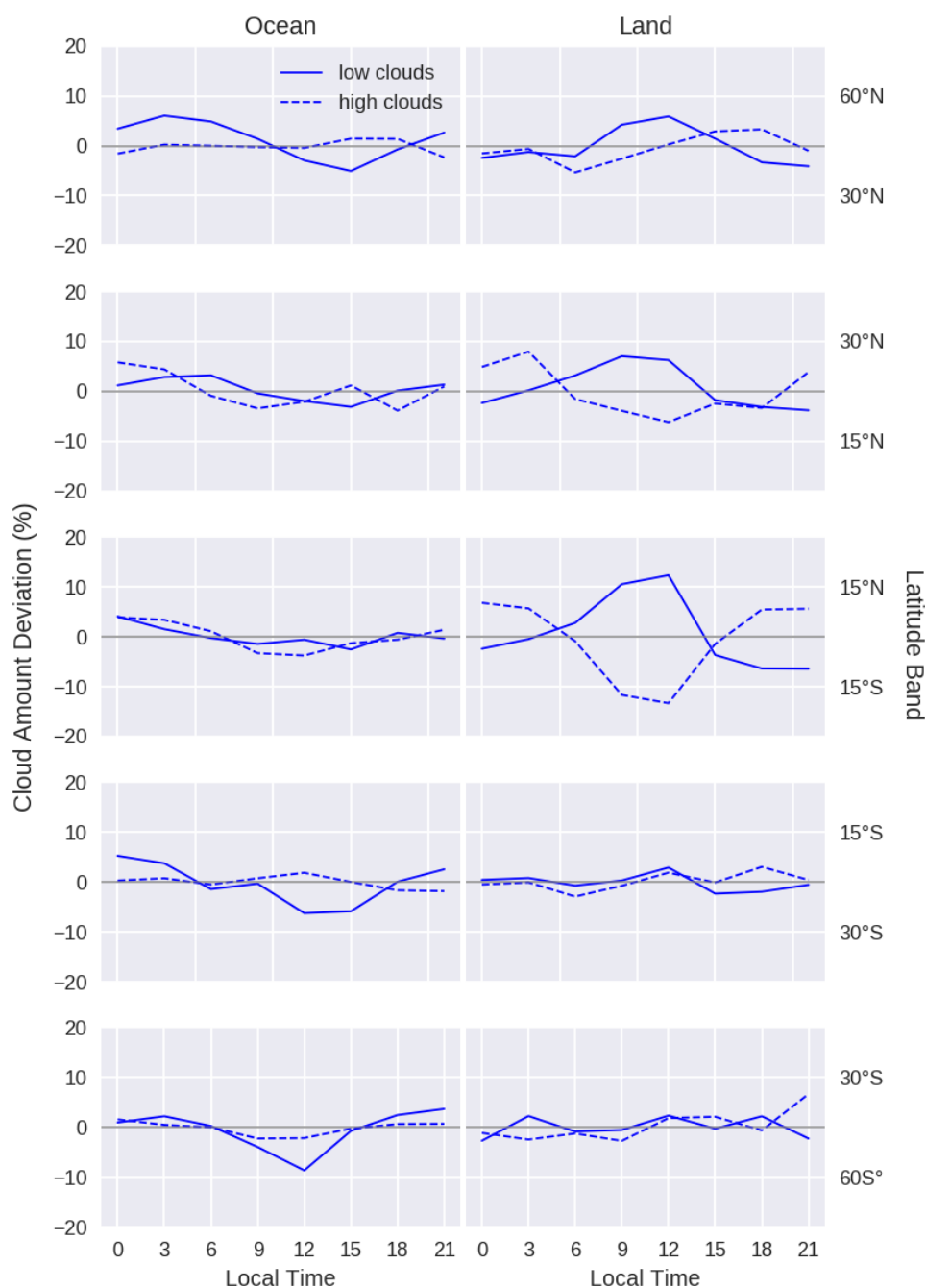


866

867 Figure 5: Diurnal cycle of the cloud fraction profiles observed by CATS over different
868 continents a) NH America, b) Europe, c) China, d) NH Africa, e) SH America, f) SH Africa, g)
869 Australia, averaged over the summer seasons (JJA in the North Hemisphere, DJF in the South
870 Hemisphere) from 2015 to 2017. For each region we considered all profiles sampled over
871 land within the boundaries shown by the inset map. CF over Europe do not extend as high
872 altitudes as the rest, as it is the only region that do not include part of the Tropical band.



873



874

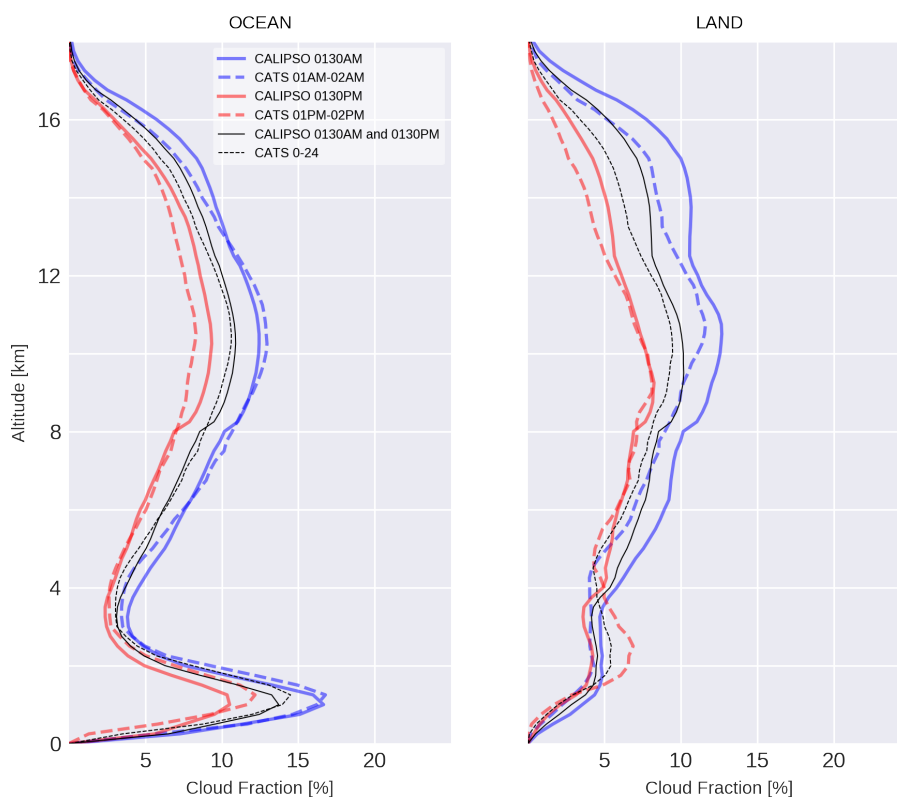
875 Figure 6: Mean diurnal variations of low-level (solid line) and high-level (dotted line) cloud
 876 amounts (%) every 3 hours in five zonal bands over ocean (left) and land (right) in JJA from



877 CATS for the period 2015-2017. Plots (a-f) are presented in a similar way as Figure 11 in RS99
878 for comparison.
879



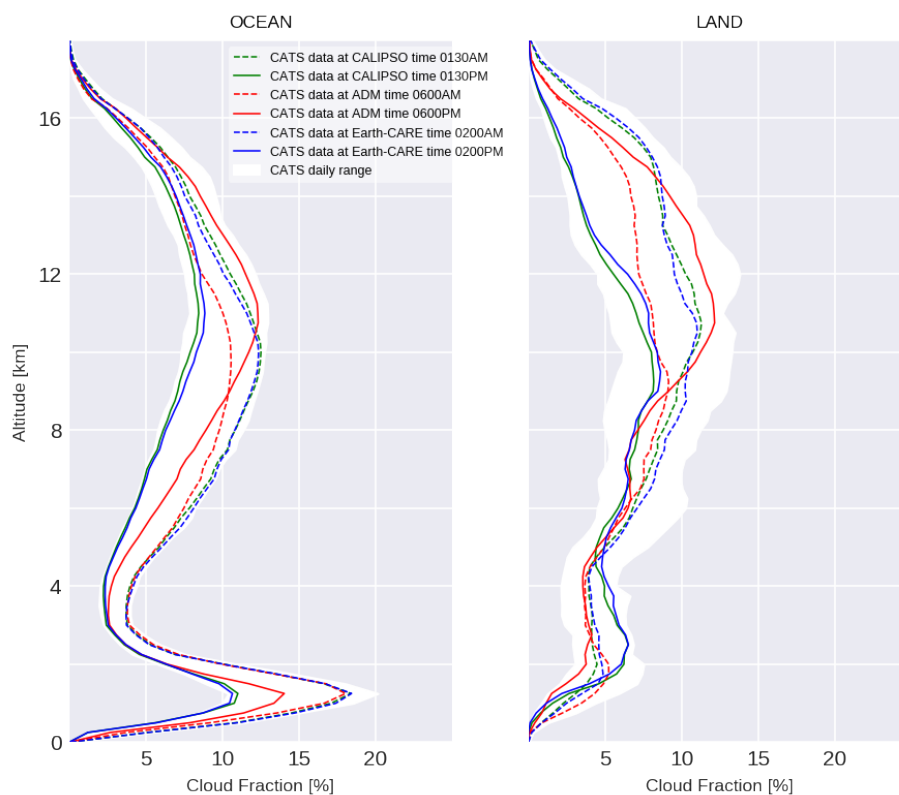
JJA 2015-2016-2017 51S-51N



880

881 Figure 7: Vertical Profiles of Cloud Fraction observed by CALIPSO (full line) and CATS (dashed
882 line) between $\pm 51^\circ$ around 0130AM (blue), 0130PM (red) and at all times (black), over ocean
883 (left) and land (right). Measurements were weighted based on the latitude at which they
884 were made, to account for the different zonal sampling distributions of both instruments.
885 CALIOP cloud profiles were built using cloud layers from the CALIPSO v4.10 level 2, 5-km
886 cloud layer product. Only layers with a Cloud/Aerosol Discrimination score (CAD_Score)
887 above 0.7 were considered to build the CALIOP profiles, and layers with a
888 Feature_Type_Score above 5 were considered to build the CATS profiles. For both
889 instruments, we used JJA observations from 2015 to 2017.

890



891

892 Figure 8: Mean Cloud fraction profiles observed by CATS at the overpass local time of the

893 sun-synchronous space lidars (CALIPSO and the A-train 01:30UTC, ADM 06:00UTC, Earth-

894 CARE 02:00UTC) compared to the envelope of the whole cloud fraction profile diurnal cycle

895 observed by CATS (white), averaged between $\pm 51^\circ$ over ocean (left) and land (right).

896 CALIPSO and Earth-CARE are dedicated to clouds and aerosols studies, while ADM is primarily

897 dedicated to wind measurements in non-cloudy conditions. We used CATS observations

898 during JJA from 2015 to 2017.



899 **Appendix A - CATS sampling compared to CALIPSO**

900

901 Figure A1 shows the number of profiles sampled by CATS divided by the number of profiles
902 sampled by CALIOP in the same 2° latitude band, when aggregated over two successive JJA
903 seasons (2015-2016). The red line considers all CATS profiles, while the green line only
904 considers CATS profiles sampled roughly around the local time sampled by CALIOP -- i.e. the
905 green line shows CATS measurements made at the same local time as CALIOP. These results
906 are based on CALIOP's v4.10 level 2, 5-km cloud layer product and CATS's v2.05 level 2, 5-km
907 cloud layer product.

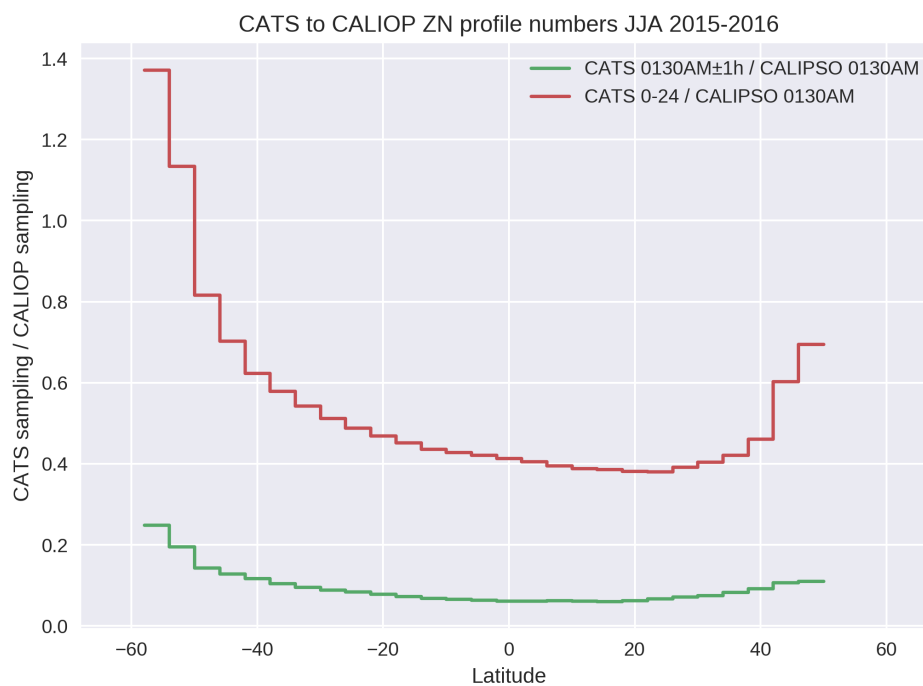
908

909 The orbital differences between the CALIPSO satellite and the ISS mean that CATS samples
910 generally less profiles than CALIOP, with a 0.4 minimum ratio near 20°N during the JJA
911 period. At that latitude, CALIOP samples more than double the number of profiles sampled
912 by CATS, when considering all local times. When considering only profiles sampled by CATS
913 at the same local time as CALIOP, the ratio drops to 0.1, meaning CALIOP's sampling is ten
914 times better the one from CATS. This ratio means that CATS data need to be aggregated over
915 long periods for any comparison between both instruments to be meaningful.

916

917 When considering high latitudes (50° and above), CATS sampling improves significantly, up
918 to the point where it gets better than CALIOP's: the CATS to CALIOP sampling ratio reaches
919 1.4 for latitudes above 50°S.

920



921

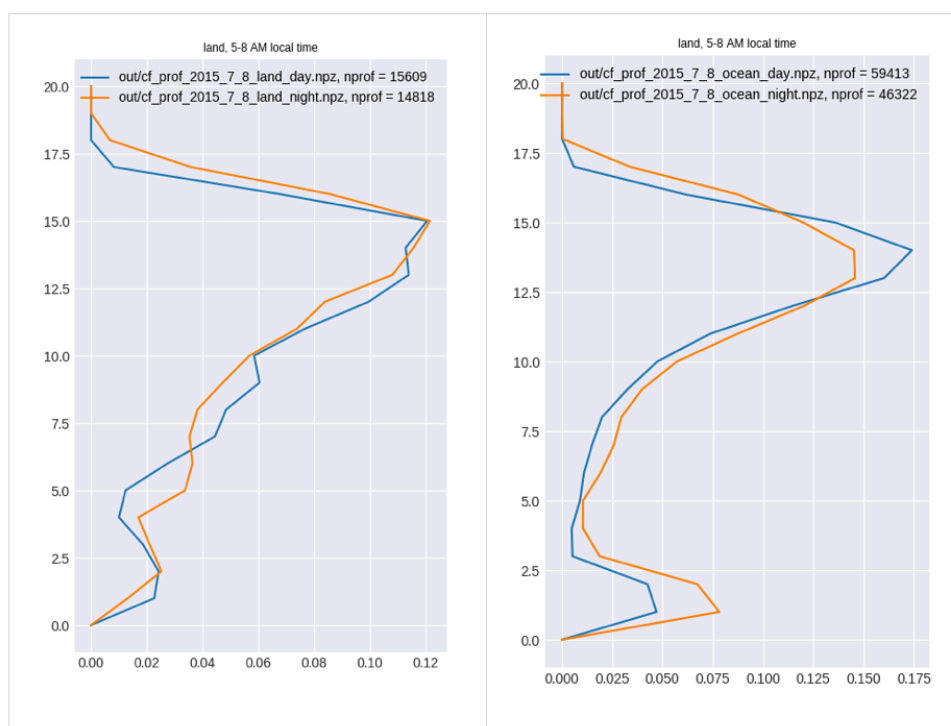
922 Fig. A1: ratio of the number of profiles seen by CATS and CALIOP in 2° latitude bands over
923 the JJA periods of 2015 and 2016.



924 **Appendix B - Continuity of CATS cloud detections according to solar pollution**

925

926 Fig. A2 shows Cloud Fraction profiles observed by CATS over land (left) and ocean (right)
927 between 5 and 8 AM local time in nighttime (orange) and daytime (blue) conditions. Here
928 we show that cloud detections made using data acquired by CATS either in daytime (sunlit)
929 conditions (blue) or nighttime conditions (orange) leads to similar cloud fraction profiles.
930 This suggests that CATS cloud detections are consistent in both conditions and that the
931 instrument can provide a continuously stable record of cloud detections throughout the day.
932



933

934 Fig. A2. Profiles of Cloud Fraction observed by CATS over land (left) and ocean (right)
935 between 5 and 8AM local time (JJA 2015–2016) in nighttime (orange) and daytime (blue)
936 conditions.

937

938 **Appendix C - Sampling bias due to CATS lidar attenuation, by region**

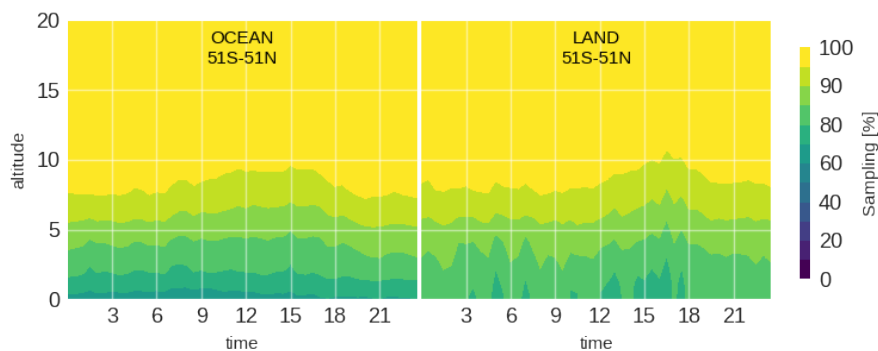
939

940 Figures A3 to A7 below document how the CATS sampling get relatively degraded from high
941 to low altitudes due to the attenuation of the laser light as it gets progressively scattered by
942 atmospheric components, for the various regions described in the main article. Sampling is
943 reported relative to its initial value of 100% at high altitudes, where no attenuation has yet
944 occurred.

945

946 Fig. A3 - Vertical sampling over ocean (left) and land (right) between 51°S and 51°N (same
947 data as in Fig. 1 in the main article)

948



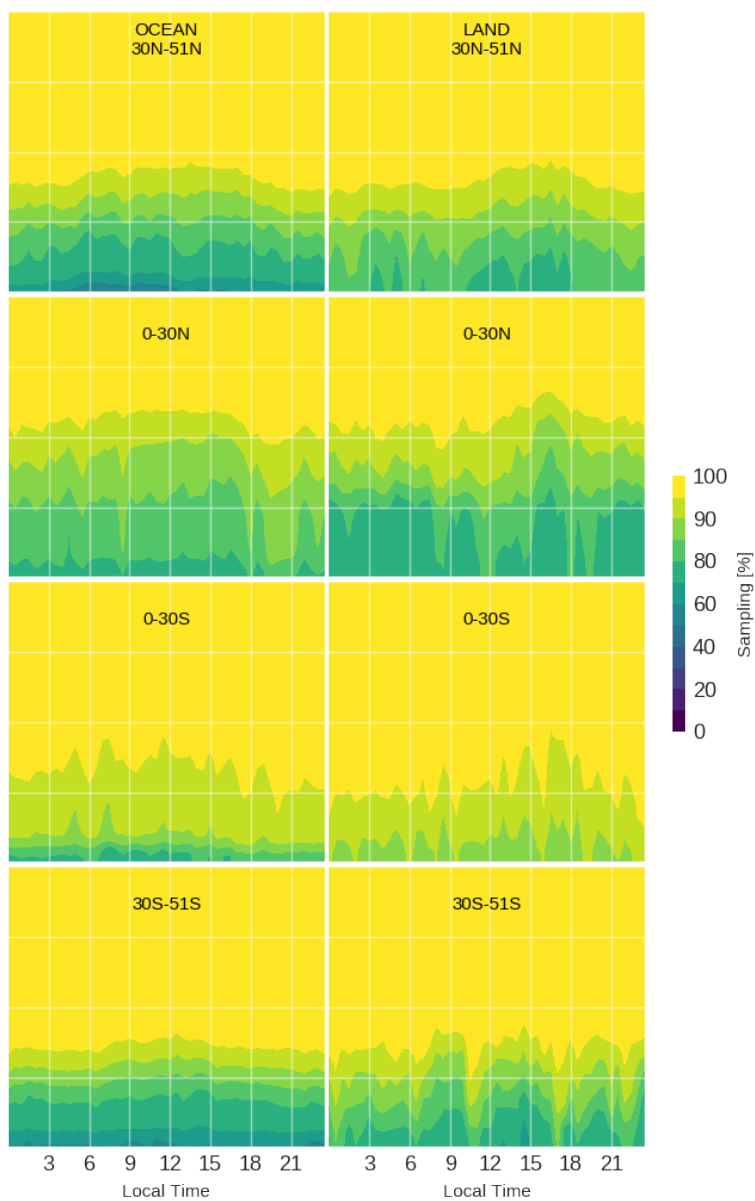
949

950

951



952 Fig. A4 - Vertical sampling over ocean (left) and land (right) in latitude bands during JJA
953 (same data as in Fig. 2 in the main article)

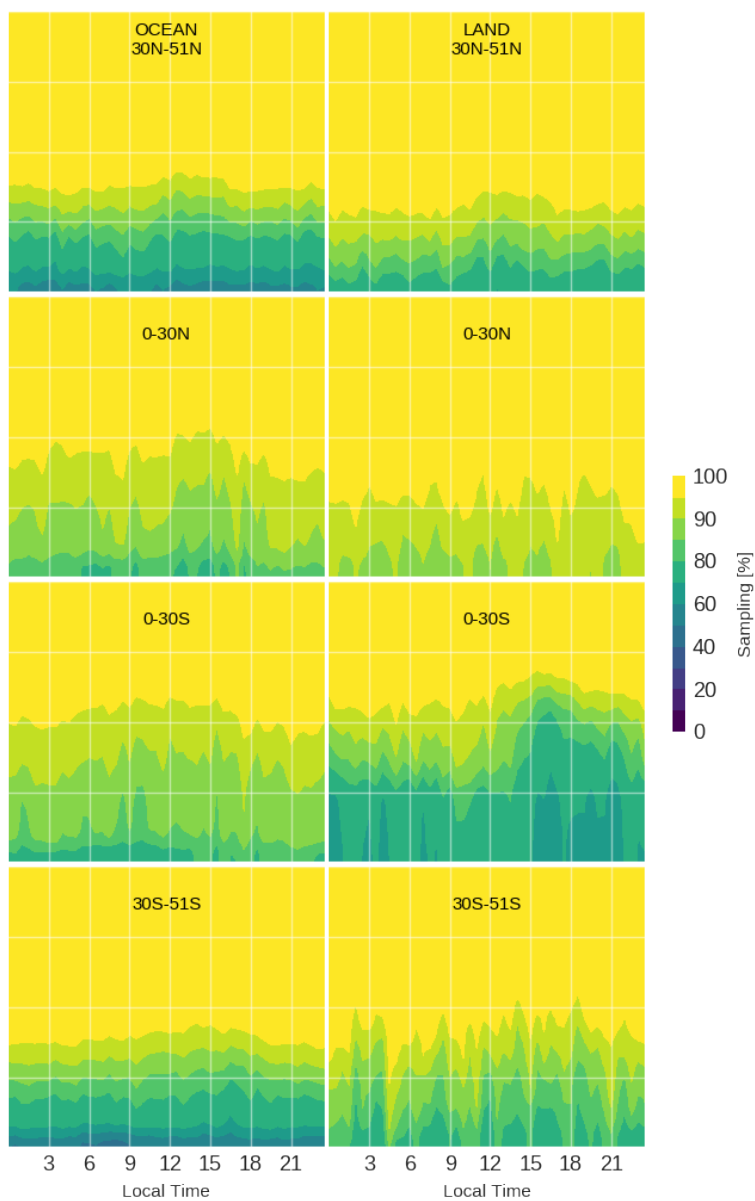


954

955



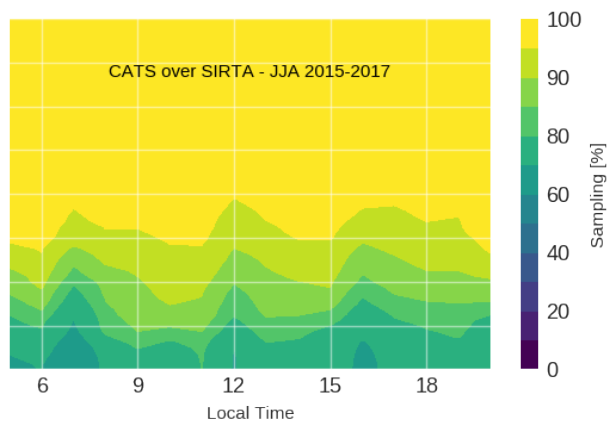
956 Fig. A5 - Vertical sampling over ocean (left) and land (right) in latitude bands during DJF
957 (same data as in Fig. 3 in the main article)



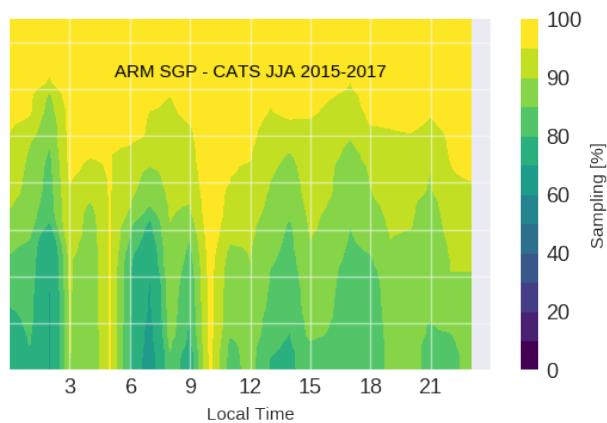
958
959
960



961 Fig A6 - Vertical sampling of the CATS lidar over the SIRTA ground-based site (top) and over
962 the ARM SGP site (bottom), same data as in Fig. 4 in the main article



963



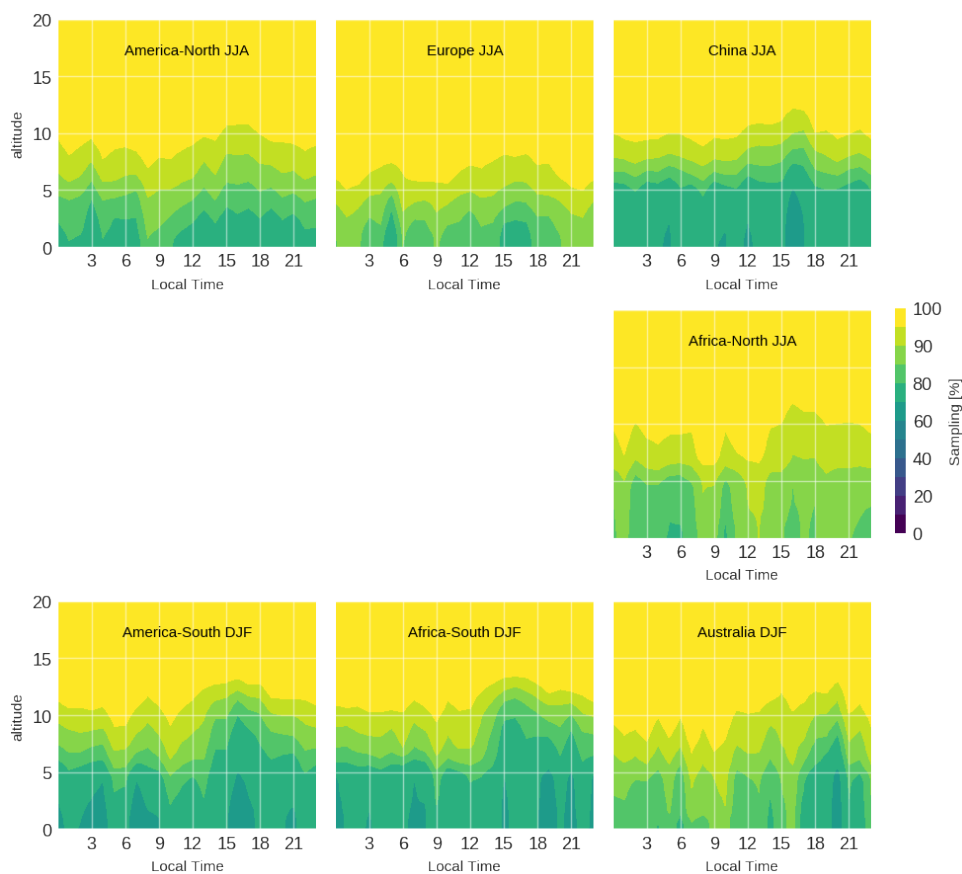
964

965

966



967 Fig. A7 - Vertical sampling over the regions considered in Fig. 5 from the main paper, during
968 JJA.
969



970
971